



# **NAVAL POSTGRADUATE SCHOOL**

**MONTEREY, CALIFORNIA**

## **THESIS**

**A MICROSTRUCTURAL AND MECHANICAL PROPERTY  
CORRELATION OF FRICTION STIR PROCESSED  
NICKEL ALUMINUM BRONZE**

by

Robert A Williams

September 2004

Thesis Advisor:

Terry R. McNelley

**Approved for public release; distribution is unlimited**

THIS PAGE INTENTIONALLY LEFT BLANK

<b>REPORT DOCUMENTATION PAGE</b>			<i>Form Approved OMB No. 0704-0188</i>	
Public reporting burden for this collection of information is estimated to average 1 hour per response, including the time for reviewing instruction, searching existing data sources, gathering and maintaining the data needed, and completing and reviewing the collection of information. Send comments regarding this burden estimate or any other aspect of this collection of information, including suggestions for reducing this burden, to Washington headquarters Services, Directorate for Information Operations and Reports, 1215 Jefferson Davis Highway, Suite 1204, Arlington, VA 22202-4302, and to the Office of Management and Budget, Paperwork Reduction Project (0704-0188) Washington DC 20503.				
<b>1. AGENCY USE ONLY (Leave blank)</b>		<b>2. REPORT DATE</b> September 2004	<b>3. REPORT TYPE AND DATES COVERED</b> Master's Thesis	
<b>4. TITLE AND SUBTITLE:</b> A Microstructural and Mechanical Property Correlation of Friction Stir Processed Nickel Aluminum Bronze			<b>5. FUNDING NUMBERS</b>	
<b>6. AUTHOR(S)</b> Williams, Robert A.				
<b>7. PERFORMING ORGANIZATION NAME(S) AND ADDRESS(ES)</b> Naval Postgraduate School Monterey, CA 93943-5000			<b>8. PERFORMING ORGANIZATION REPORT NUMBER</b>	
<b>9. SPONSORING /MONITORING AGENCY NAME(S) AND ADDRESS(ES)</b> Defense Advanced Research Project Agency (DARPA): Dr. Leo Christodoulou DARPA/DSO, 3701 North Fairfax Drive, Arlington, VA 22203-1714			<b>10. SPONSORING/MONITORING AGENCY REPORT NUMBER</b>	
<b>11. SUPPLEMENTARY NOTES</b> The views expressed in this thesis are those of the author and do not reflect the official policy or position of the Department of Defense or the U.S. Government.				
<b>12a. DISTRIBUTION / AVAILABILITY STATEMENT</b> Approved for public release; distribution is unlimited			<b>12b. DISTRIBUTION CODE</b>	
<b>13. ABSTRACT (maximum 200 words)</b> Friction Stir Processing (FSP) is novel technique for localized modification of the surface layer of materials. FSP produces high local strains, strain rates and local temperatures that are 0.8 - 0.9 T <sub>m</sub> , where T <sub>m</sub> is the melting point. The processing enhances the microstructural and mechanical properties of materials through intense plastic deformation. This thesis examines the microstructure and tensile properties in FSP'ed Nickel Aluminum Propeller Bronze (NAB) as a function of position in the stir zone using a unique miniature tensile sample design. Test materials were single and multi-pass FSP runs from both 6 mm and 13 mm tools. Tensile ductility was observed to increase from 11 percent to more than 30 percent elongation to fracture at locations along the center of the stir zone. Yield and ultimate strengths also increased two-fold. These improved properties were associated with the formation of Widmanstätten $\alpha$ and fine, equiaxed $\alpha$ at peak temperatures of approximately 1000 <sup>0</sup> C in these locations. Some locations in the heat affected zone (HAZ) or thermomechanically affected zone (TMAZ) exhibited ductilities below that of as-cast material. Such regions had microstructures that contained a dark-etching constituent formed by cooling after being heated to approximately 800 <sup>0</sup> C.				
<b>14. SUBJECT TERMS</b> Friction Stir Processing, Ni Al Bronze, Microstructure, Mechanical Properties.			<b>15. NUMBER OF PAGES</b> 71	
			<b>16. PRICE CODE</b>	
<b>17. SECURITY CLASSIFICATION OF REPORT</b> Unclassified	<b>18. SECURITY CLASSIFICATION OF THIS PAGE</b> Unclassified	<b>19. SECURITY CLASSIFICATION OF ABSTRACT</b> Unclassified	<b>20. LIMITATION OF ABSTRACT</b> UL	

THIS PAGE INTENTIONALLY LEFT BLANK

**Approved for public release; distribution is unlimited**

**A MICROSTRUCTURAL AND MECHANICAL PROPERTY CORRELATION  
OF FRICTION STIR PROCESSED NICKEL ALUMINUM BRONZE**

Robert A. Williams  
Lieutenant Commander, United States Navy  
B.S., Norfolk State University, 1995

Submitted in partial fulfillment of the  
requirements for the degree of

**MASTER OF SCIENCE IN MECHANICAL ENGINEERING**

from the

**NAVAL POSTGRADUATE SCHOOL  
September 2004**

Author: Robert A. Williams

Approved by: Terry R. McNelley  
Thesis Advisor

Anthony J. Healey  
Chairman, Department of Mechanical and Astronautical  
Engineering

THIS PAGE INTENTIONALLY LEFT BLANK

## ABSTRACT

Friction Stir Processing (FSP) is novel technique for localized modification of the surface layer of materials. FSP produces high local strains, strain rates and local temperatures that are 0.8 - 0.9  $T_m$ , where  $T_m$  is the melting point. The processing enhances the microstructural and mechanical properties of materials through intense plastic deformation. This thesis examines the microstructure and tensile properties in FSP'ed Nickel Aluminum Propeller Bronze (NAB) as a function of position in the stir zone using a unique miniature tensile sample design. Test materials were single and multi-pass FSP runs from both 6 mm and 13 mm tools. Tensile ductility was observed to increase from 11 percent to more than 30 percent elongation to fracture at locations along the center of the stir zone. Yield and ultimate strengths also increased two-fold. These improved properties were associated with the formation of Widmanstätten  $\alpha$  and fine, equiaxed  $\alpha$  at peak temperatures of approximately 1000<sup>0</sup>C in these locations. Some locations in the heat affected zone (HAZ) or thermomechanically affected zone (TMAZ) exhibited ductilities below that of as-cast material. Such regions had microstructures that contained a dark-etching constituent formed by cooling after being heated to approximately 800<sup>0</sup>C.

THIS PAGE INTENTIONALLY LEFT BLANK

# TABLE OF CONTENTS

<b>I.</b>	<b>INTRODUCTION.....</b>	<b>1</b>
<b>A.</b>	<b>OVERVIEW .....</b>	<b>1</b>
<b>B.</b>	<b>FRICTION STIR PROCESSING .....</b>	<b>1</b>
<b>C.</b>	<b>NICKEL ALUMINUM BRONZE (NAB) .....</b>	<b>4</b>
<b>1.</b>	<b>NAB Microstructure.....</b>	<b>6</b>
<b>D.</b>	<b>PREVIOUS FINDINGS .....</b>	<b>7</b>
<b>1.</b>	<b>Rolling Studies.....</b>	<b>7</b>
<b>2.</b>	<b>Associated Research.....</b>	<b>8</b>
<b>E.</b>	<b>OBJECTIVE .....</b>	<b>9</b>
<b>II.</b>	<b>EXPERIMENTAL PROCEDURES AND TESTING.....</b>	<b>11</b>
<b>A.</b>	<b>SAMPLE AND PROCEDURE DEVELOPMENT.....</b>	<b>11</b>
<b>B.</b>	<b>MATERIAL &amp; COMPOSITION.....</b>	<b>13</b>
<b>C.</b>	<b>MICROSCOPY.....</b>	<b>15</b>
<b>1.</b>	<b>Sample Preparation .....</b>	<b>15</b>
<b>2.</b>	<b>Optical Microscopy .....</b>	<b>16</b>
<b>D.</b>	<b>TENSILE SAMPLING.....</b>	<b>16</b>
<b>1.</b>	<b>Sample Preparation .....</b>	<b>16</b>
<b>2.</b>	<b>Tensile Testing.....</b>	<b>17</b>
<b>III.</b>	<b>RESULTS AND DISCUSSION .....</b>	<b>19</b>
<b>A.</b>	<b>TENSILE TEST DATA.....</b>	<b>19</b>
<b>B.</b>	<b>MICROSTRUCTURE PROPERTY CORRELATIONS .....</b>	<b>26</b>
<b>1.</b>	<b>Areas of High Ductility .....</b>	<b>26</b>
<b>2.</b>	<b>Areas of Low Ductility.....</b>	<b>27</b>
<b>3.</b>	<b>Ductility Contours.....</b>	<b>30</b>
<b>C.</b>	<b>CORRELATION OF DUCTILITY WITH MICROSTRUCTURE.....</b>	<b>34</b>
<b>1.</b>	<b>High Ductility .....</b>	<b>34</b>
<b>2.</b>	<b>Low Ductility .....</b>	<b>35</b>
<b>IV.</b>	<b>CONCLUSIONS AND RECOMMENDATIONS.....</b>	<b>37</b>
<b>A.</b>	<b>CONCLUSIONS .....</b>	<b>37</b>
<b>B.</b>	<b>RECOMMENDATIONS FOR FUTURE RESEARCH.....</b>	<b>37</b>
	<b>APPENDIX A – STRESS VS. STRAIN PLOTS.....</b>	<b>39</b>
<b>A.</b>	<b>740 SERIES .....</b>	<b>39</b>
<b>B.</b>	<b>741 SERIES .....</b>	<b>40</b>
<b>C.</b>	<b>751 SERIES .....</b>	<b>41</b>
<b>D.</b>	<b>754 SERIES .....</b>	<b>42</b>
<b>E.</b>	<b>858 SERIES .....</b>	<b>43</b>
<b>F.</b>	<b>859 SERIES .....</b>	<b>44</b>
<b>G.</b>	<b>BASE METAL SERIES .....</b>	<b>45</b>
	<b>APPENDIX B – MESH AND CONTOUR PLOTS .....</b>	<b>47</b>

A.	740 SERIES .....	47
B.	741 SERIES .....	48
C.	751 SERIES .....	49
D.	754 SERIES .....	50
E.	858 SERIES .....	51
F.	859 SERIES .....	52
LIST OF REFERENCES .....		53
INITIAL DISTRIBUTION LIST .....		55

## LIST OF FIGURES

Figure 1.	Schematic illustration of FSP (After [4]).....	2
Figure 2.	Example of the FSP region. ....	3
Figure 3.	Examples of Area Processing .....	4
Figure 4.	Typical Raster Patterns .....	4
Figure 5.	Area Processing of a Marine Propeller (From [13]) .....	6
Figure 6.	Microstructures created in NAB by friction stir processing (From [13]) .....	7
Figure 7.	Ductility and strength Vs. temperature graphs (From [16]) .....	8
Figure 8.	Miniature sample dimensions in millimeters.....	11
Figure 9.	Tensile blank orientation and numbering .....	12
Figure 10.	Representation of a single sample location within the stir zone .....	13
Figure 11.	FSP Material .....	14
Figure 12.	6mm and 13mm FSP tools (From [13]).....	15
Figure 13.	Aligning mini sample in grips.....	18
Figure 14.	Typical stress strain plots; the depth below the surface is indicated for each sample.....	20
Figure 15.	FSP 754 UTS mesh plot.....	23
Figure 16.	FSP 754 yield strength plot.....	24
Figure 17.	FSP 754 ductility plot .....	25
Figure 18.	Area of highest ductility in FSP 754 and its microstructure.....	26
Figure 19.	Areas of high ductility and associated microstructures from FSP 741 .....	27
Figure 20.	Montage, micrograph and fractography of FSP 740.....	28
Figure 21.	Montage, micrograph and fractography of FSP 754 (blank #1) .....	29
Figure 22.	Montage, micrograph and fractography of FSP 754 (blank #3) .....	29
Figure 23.	Montage, micrograph and fractography of FSP 754 (blank #2) .....	30
Figure 24.	FSP 858 ductility mesh plot.....	31
Figure 25.	FSP 858 ductility contour plot .....	32
Figure 26.	FSP 754 ductility contour plot .....	33

THIS PAGE INTENTIONALLY LEFT BLANK

## LIST OF TABLES

Table 1.	Composition (wt.%) of UNS C95800 NAB (Adapted from [17]).....	14
Table 2.	FSP process histories (See Figure 4a for multi-pass illustration) .....	15
Table 3.	Mechanical Polishing Schedule (From [16]) .....	16
Table 4.	FSP Yield and Ultimate Tensile Strengths, with Elongation (Base Metal, 858 & 859) .....	21
Table 5.	Yield and Ultimate Tensile Strengths, with Elongation (754, 740, 741, & 751) .....	22

THIS PAGE INTENTIONALLY LEFT BLANK

## **ACKNOWLEDGMENTS**

The author would like to thank the Defense Advanced Research Projects Agency and Dr. Leo Christodoulou for support of this research, and Mr. Murray Mahoney and his crew at the Rockwell Scientific Center, Thousand Oaks, CA for their material support.

Special thanks to Professor Terry McNelley for sharing his knowledge, insights and vision. It was a pleasure working with you.

Thanks to Dr. Chanman Park for hardware support, Dr. Alex Zhilyaev for software support and Dr. Keiichiro Oishi for microscopy support and assistance. I am greatly indebted to all of you.

No amount of thanks can express my gratitude and that of all the future engineering materials students to LT Frank Pierce, USCG for restoring the Charmilles Andrew EF630 electric discharge machine (EDM). Our lives are now easier.

To Romy with love - Thank you for enduring my absence once again. All that I am or will ever be is a testament to your unfailing love and support. You are The Wife of Noble Character.

THIS PAGE INTENTIONALLY LEFT BLANK

# **I. INTRODUCTION**

## **A. OVERVIEW**

The qualities of strength, ductility and toughness have been long sought in materials for structural applications, and obtained to varying degrees through numerous processing methods. Friction Stir Processing (FSP) is one of the newest methods and provides highly selective microstructural modification of material without producing significant distortion to the original shape. In a program funded by the Defense Advanced Research Projects Agency, the research being conducted at the Naval Postgraduate School in collaboration with other program participants aims to provide the microstructural analysis and related mechanical characterization studies. Altogether, the program will establish the foundation necessary to help commercialize FSP, and, in particular, for the technique to be used in the post processing of U.S. Navy propeller castings. A thorough understanding of the mechanical and microstructural properties in relation to thermomechanical history, and with respect to process parameters, is essential for meeting this objective.

## **B. FRICTION STIR PROCESSING**

Friction stir processing (FSP) is an emerging metal working technology that can provide localized modification and control of microstructures in near-surface layers of processed metallic components [1-3]. FSP uses the same methodology as friction stir welding (FSW). FSW is a solid state joining process invented at The Welding Institute (TWI) in 1991 as a technique for joining Al alloys that are difficult to fusion weld [4]. FSP modifies local microstructures in a material but with the absence of joining. A schematic illustration of FSP is shown in Figure 1. In FSP, a specially designed, cylindrical tool is rotated and plunged into a selected area (Figure 1a). The tool has a small diameter pin with a concentric larger diameter shoulder. When plunged into the material, the rotating pin contacts the surface and rapidly heats and softens a small column of metal by frictional and adiabatic effects (Figure 1b). The tool shoulder and pin length control the penetration depth (Figure 1c).

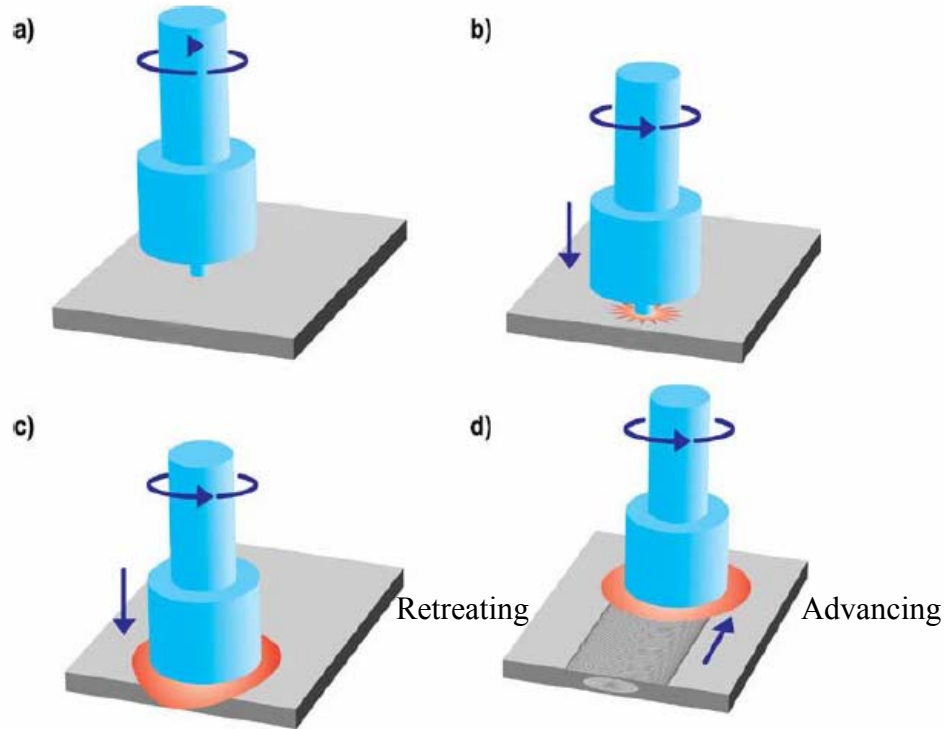


Figure 1. Schematic illustration of FSP (After [4])

FSP is considered a severe hot working process in which extreme localized strains and strain rates, as well as high temperatures are capable of transforming microstructure and mechanical properties of cast material to a wrought condition, thus significantly increasing the properties of both strength and toughness [5, 6]. The process is also characterized by steep gradients in strain, strain rate and temperature, leading as well to gradients in microstructure and properties. Secondary benefits for some materials include superplasticity effects, better weldability and improved fatigue/corrosion resistance [7].

Friction Stir process parameters and material conditions are defined with terminology commonly used in welding. In common with welding processes, FSP shares a “heat affected zone” (HAZ); however, in FSP there is also a thermomechanically affected zone (TMAZ) where localized hotworking occurs [6]. In some locations peak temperatures ( $T_{\text{peak}}$ ) reach  $> 0.9 T_{\text{melt}}$  although melting has not been observed. FSP unique terms include the “stir zone” (SZ), also known as the “stir nugget” [4-7]. The micrograph in Figure 2 shows a transverse section of FSP NiAl Bronze. This figure depicts three important zones, SZ, TMAZ and HAZ, relative to the base metal.

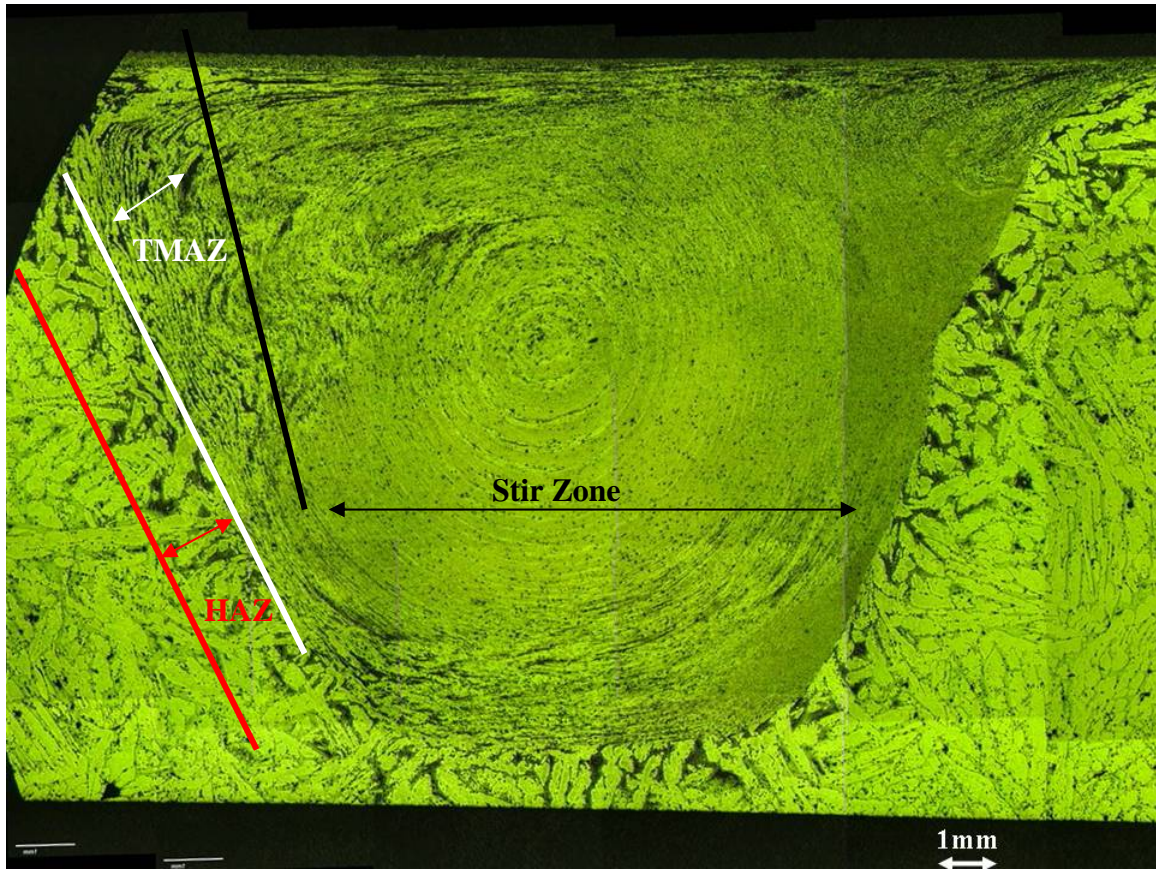
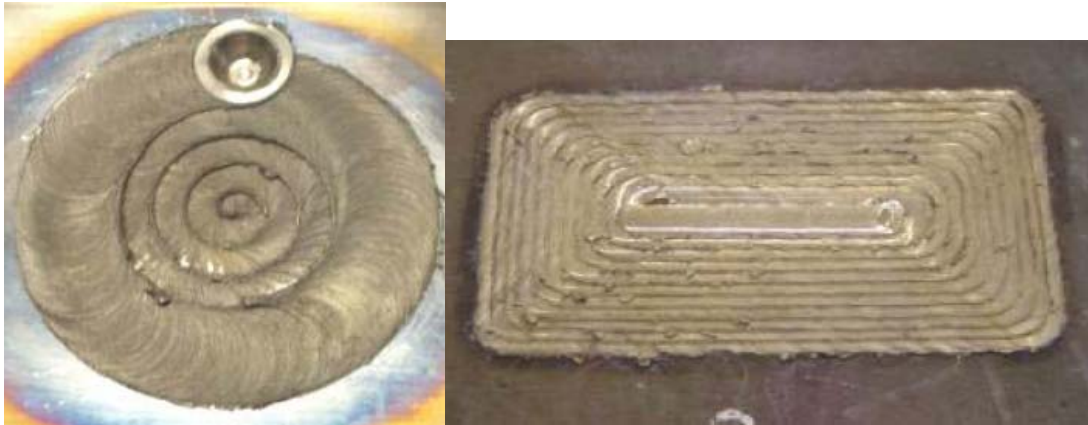


Figure 2. Example of the FSP region.

Diameters for the tool shoulders and pins vary from a few millimeters up to a few centimeters. Pin depths for these tools can range up to 100% of their largest diameter, depending on the material. The pin is always concentric to the shoulder. The tool geometry is a vital parameter in the size and shape of the SZ and the resulting flow within the stir zone. Speed of rotation is variable and is expressed in revolutions per minute (RPM). The travel direction is defined as the direction the rotational axis of the tool travels and is not restricted to straight lines. The speed or traverse rate of the tool is expressed as inches per minute (IPM). The axial force is applied inline of the rotational axis and nearly normal to the surface of the material; the alignment mismatch is because tool axis may be inclined away from the travel direction in some materials for the purpose of defect minimization. FSP can be used as an area processing method by using raster or spiral patterns as shown in Figures 3 and 4. Microstructure within the FSP material is significantly different from the advancing to the retreating side of the stir

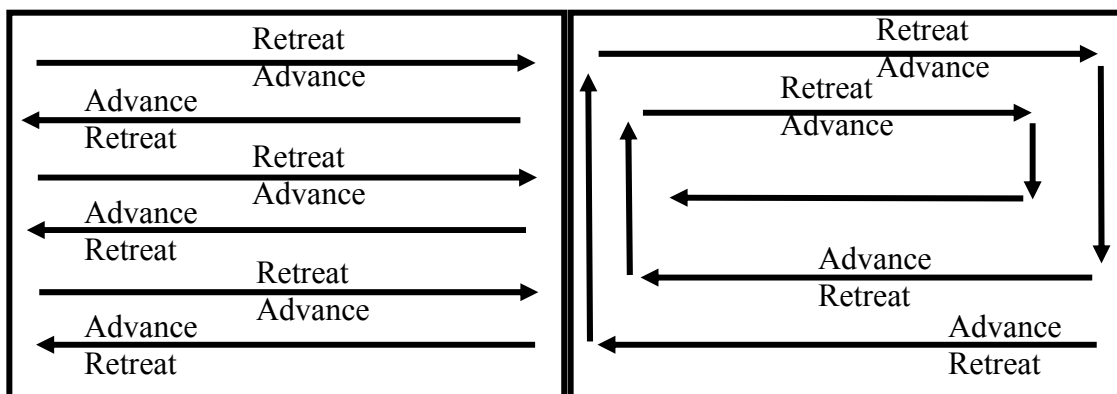
zone. On the advancing side, where tool rotation direction and travel direction are the same, the microstructure is very fine and homogeneous. On the retreating side, where tool rotation is opposite the travel direction, the microstructure is not as refined or homogeneous. Depending on tool rotation and travel direction, a number of stir zone interface combinations are possible. Typical combinations are illustrated in Figure 4.



Spiral

Raster

Figure 3. Examples of Area Processing



a) CCW Adv/Adv, Ret/Ret Pattern

b) CCW Advancing on Retreating

Figure 4. Typical Raster Patterns

### C. NICKEL ALUMINUM BRONZE (NAB)

Nickel-aluminum bronze (NAB), which, for certain compositions, is also known as “propeller bronze,” gained its popularity for marine applications because it exhibits a unique combination of properties that include moderate strength and toughness, coupled

with excellent fatigue, corrosion, cavitation and erosion resistance [8-9]. Propeller bronzes are Copper (Cu) based alloys with additions of Aluminum (Al), Nickel (Ni), Iron (Fe) and Manganese (Mn). Percentages of the alloying elements can vary, but fall under the specification ASTM B 148-78 designation C95800 [10]. Ship propeller castings and the casting process itself lowers the overall values of the mechanical properties when compared with wrought material primarily due to their large casting sizes. Propeller castings require many months of post-cast processing to render the propellers fit for service [11]. The massively thick sections in propeller casts result in very slow cooling rates [12]. Temperature gradients are shallow and cooling times from pouring temperatures to ambient temperature are often more than one week, which correspond to cooling rates of  $10^{-3}\text{C}\cdot\text{s}^{-1}$ ). Investigations into the effects of slow cooling in propeller casts have shown that degradation in properties can be directly attributed to related phase changes in conjunction with grain coarsening [8, 12]. Heat treatments have been attempted to mitigate the phase structure changes and segregation effects. In general, heat treatments can alter the material microstructure to obtain more desirable properties but such treatments do not remove other casting defects such as porosity [8, 12]. The treatments themselves have also been noted to promote an overall decrease in ductility [8]. Surface and sub-surface porosity remains an issue and is currently repaired with costly inspection, weld repair and re-inspection process. Welding repairs to correct porosity currently use an area welding technique known as “buttering” that can introduce further thermal stress and microstructural changes [11]. This repetitive method for cast porosity repair leads to times up to 18 months in propeller fabrication. In comparison to this method, FSP can be applied using a rastering method than can be conducted to either selectively treat regions or the entire cast surface. This is illustrated in figure 5. Aside from the mechanical property increases, the advantage that FSP offers is the elimination of much of the repetitive repair process associated with closing porosity. FSP has been projected to lower post-cast processing time significantly.



Figure 5. Area Processing of a Marine Propeller (From [13])

### **1. NAB Microstructure**

The four primary microstructures associated with the friction stir processing of NAB are pictured below. Microstructures within and surrounding the stir zone are lamellar (Figure 6a), fine grain (Figure 6b), Widmanstätten (Figure 6c) and as-cast (Figure 6d) [13].

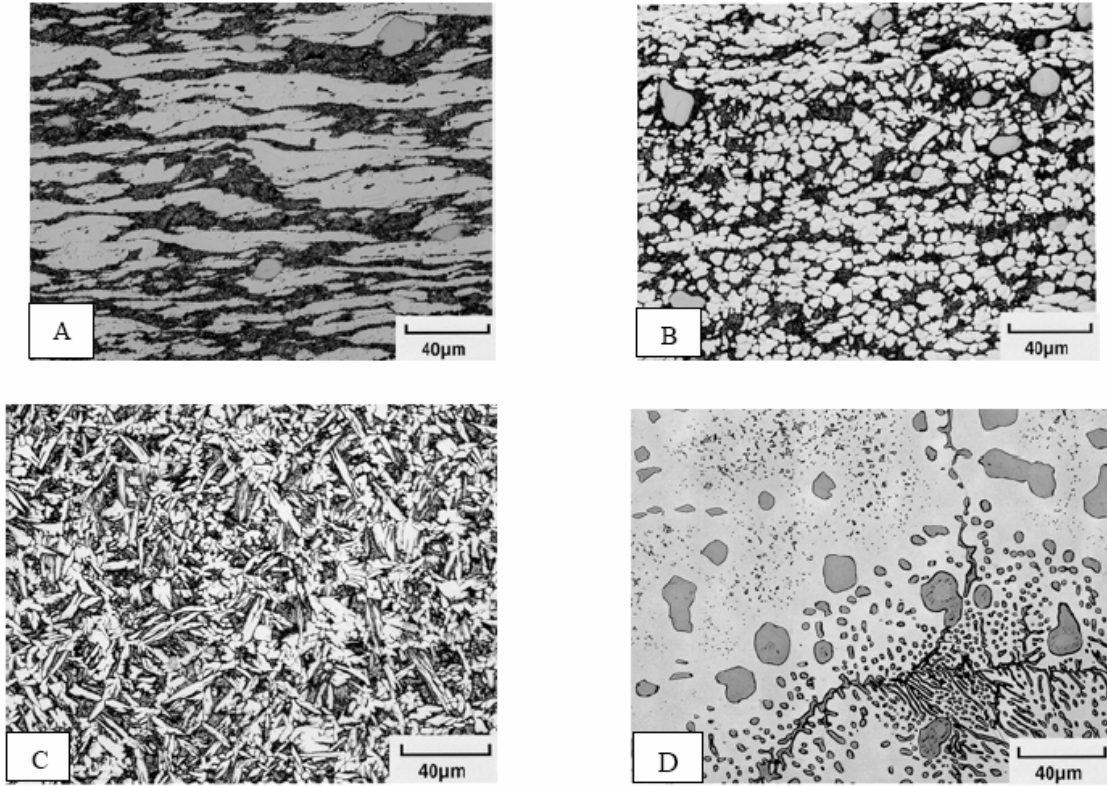


Figure 6. Microstructures created in NAB by friction stir processing (From [13])

## D. PREVIOUS FINDINGS

### 1. Rolling Studies

Previous mechanical and microstructural studies used isothermal hot rolling to provide a controlled simulation of FSP effects. The results of these studies are the building blocks of this research.

Nabach's work showed alligator cracking and extremely poor ductility at temperatures below eutectoid. He noted that this type of cracking for near eutectoid temperatures was associated with the presence of brittle  $\kappa_{iii}$  constituent particles in the microstructure [14]. Vasquez's work suggested higher FSP temperatures than previously postulated, up to 1000°C. His work also showed a linear relationship between the percentage of prior  $\beta$  transformation products and peak temperatures [15]. Pierce's work showed potential benefits of higher temps (up to 1000°C) with high strains that produced a strong and ductile Widmanstätten microstructure. At increased rolling strain, the

highest temperatures enhanced both the yield strength and ultimate tensile strength while providing the largest values of ductility. This correlates to tool parameters of high RPM coupled with low IPM. Hardness as a function of temperature for single-pass FSP and for isothermal hotworking of NAB material is relatively flat with increasing temperature despite the variations in corresponding microstructures. These results, shown in Figure 7, suggest that as process temperatures go up, both strength and ductility increase. The key to this unique effect is the linear increase with temperature of high-strength prior  $\beta$  transformation products for heating between approximately 800 °C and 1000 °C. This phenomenon is contrary to the effects of ordinary heat treating in which an increase in temperature is associated with softening and a corresponding loss in strength. Loss of ductility in heat treated NAB, as shown in Figure 7, will be a significant area of concern for overcoming reduced ductility in FSP material. Of primary note was that Widmanstätten  $\alpha$  is both strong and ductile, and is produced at temperatures above 950 °C with large deformation followed by moderate cooling rates [16].

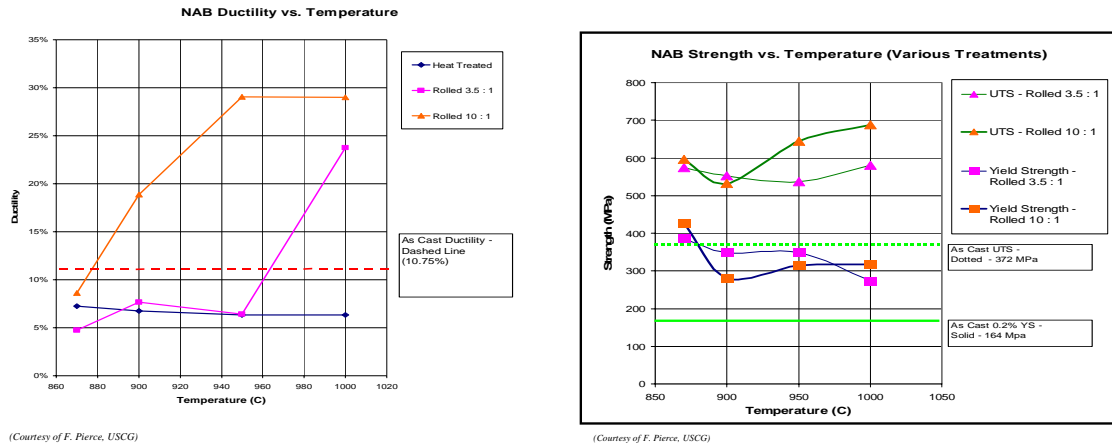


Figure 7. Ductility and strength Vs. temperature graphs (From [16])

## 2. Associated Research

Similar mechanical and microstructure studies are concurrently being performed at Rockwell Science Center and the University of Missouri. Rockwell Science Center observed infrequent but troubling occurrences of decreased ductility in processed material [13].

At the University of Missouri, R. A. Mishra has been using mini-tensile specimens for his research [13]. His success with these mini-samples led to the idea of testing the microstructure and property gradients through the stir zone. Gradients in microstructure may lead to undesirable or unexpected properties and that these gradients should be thoroughly investigated.

#### **E. OBJECTIVE**

The objective of this research is to correlate mechanical properties with the various microstructures of Friction Stir Processed NAB. Clearly, because the stir zone dimensions are a function of tool geometry, a large tensile sample may not provide an adequate representation of the processed material. A smaller sample will provide a more specific representation of the varying microstructures and properties contained within the stir zone and potentially highlight both desirable and undesirable microstructures.

In order to accomplish the goal of conducting small tensile sample to testing to obtain precise local mechanical properties, a suitably small sample must be developed that will provide reliable data. The sample size must not be so small that it can be easily deformed between manufacture and actual testing. Additionally, a precise method of sample location indexing must be developed so that the mechanical properties from each tensile sample can be associated with its corresponding microstructure.

Therefore, this research is divided into three parts. The first part was to develop a suitable sample geometry, manufacture and indexing method. The second was to obtain FSP material of various process histories and perform testing in accordance with the indexing schedule. Finally, the third step was to collect, collate, and interpret the data.

THIS PAGE INTENTIONALLY LEFT BLANK

## II. EXPERIMENTAL PROCEDURES AND TESTING

### A. SAMPLE AND PROCEDURE DEVELOPMENT

Test procedures were developed consistent with locally available equipment. No special tools or machinery would be budgeted. Available grip size and configuration was the primary limitation in sample design. The availability of a Charmilles Andrew EF630 electric discharge machine (EDM) made fabrication of most sheet-type sample geometries achievable. Therefore, the tensile sample design was simply the smallest scale version of a sub size tensile sample that would fit into the 38mm flat platen grips. Final sample dimensions are includes in Figure 8.

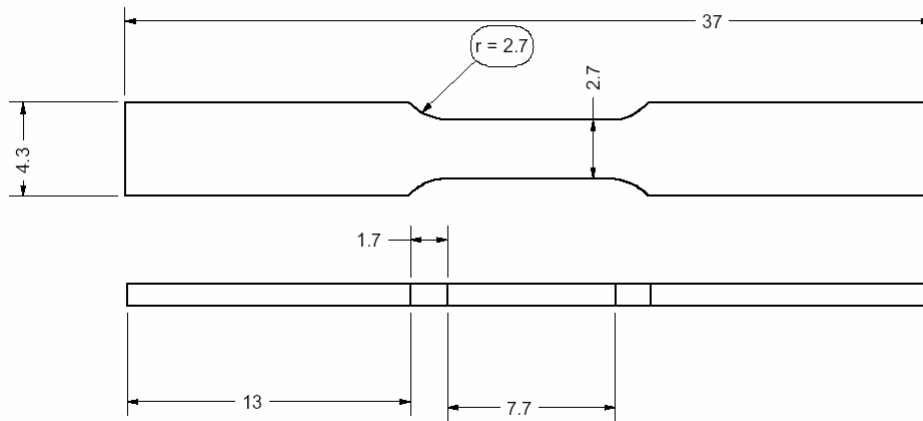


Figure 8. Miniature sample dimensions in millimeters

The sample indexing schedule was created to allow for ease of manufacture and cataloging. Samples were initially cut from the material as thick blanks that were later sectioned into 1mm thick specimens. The blanks were numbered sequentially from the top of the plate as shown in Figure 9. Thus blank 1 was from the retreating side and blank numbers increased toward the advancing side.

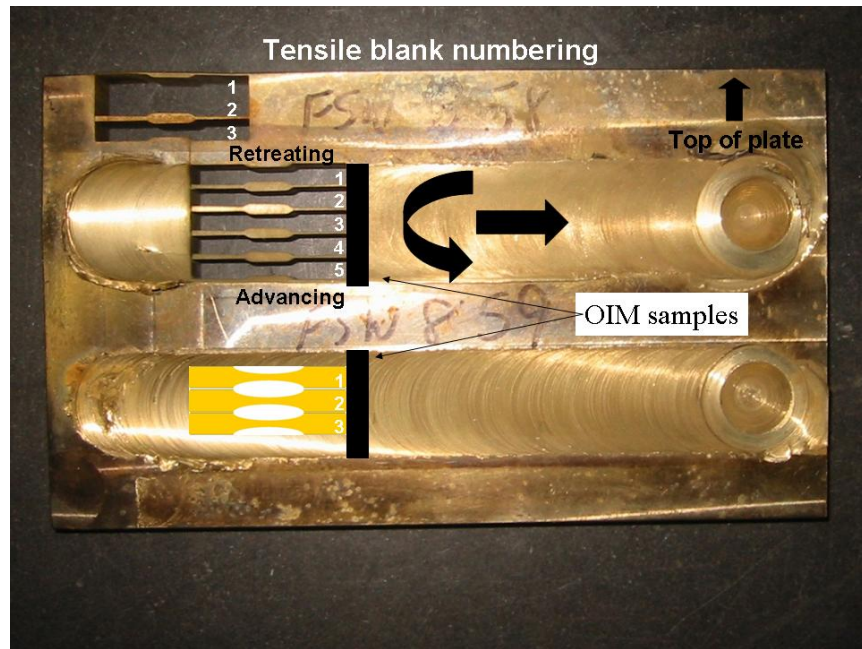


Figure 9. Tensile blank orientation and numbering

Each 1mm sample was numbered sequentially beginning at the plate surface and continuing through the depth. A typical sample number, 859-2-3, indicates the FSP number (FSP 859), sample blank number (2<sup>nd</sup> from the retreating side) and the layer number (3<sup>rd</sup> from surface), respectively. Figure 10 shows the approximate location of tensile sample 859-2-3 within the stir zone.

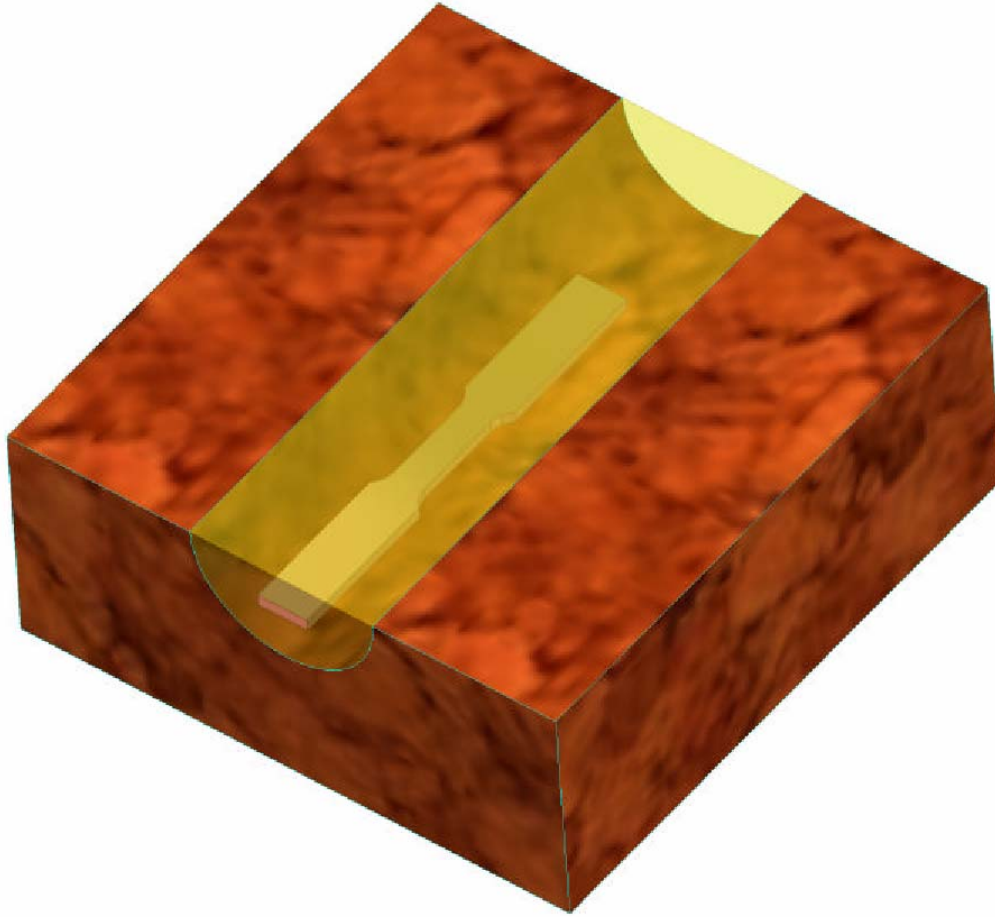


Figure 10. Representation of a single sample location within the stir zone

## **B. MATERIAL & COMPOSITION**

Friction Stir Processed material shown in Figure 11 was provided by Rockwell Scientific Corporation. The chemical analysis for this material was obtained from ANAMET Laboratories Inc., in Hayward, CA. The accepted nominal composition, composition data for material used in previous research, Alloy 1 and Alloy 2 [16], and the data for material used in the current research (designated by FSP number) are contained in Table 1. Coring and segregation effects may be responsible for the wide range of sample composition. Three of seven samples did not meet the standards established in Reference 17. Out of tolerance percentages are underlined. The material was processed using 6mm and 13 mm stepped spiral tools similar to those shown in Figure 12. Table 2 summarizes the FSP parameters used for each run.

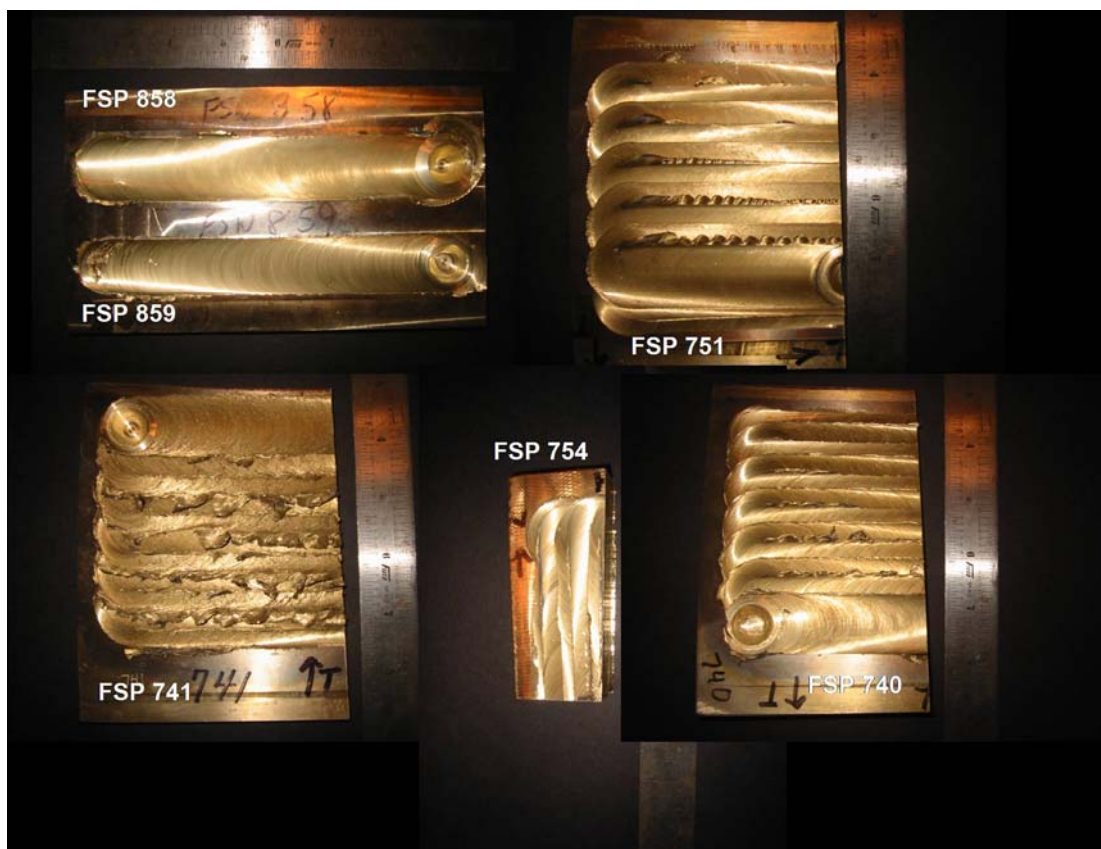


Figure 11. FSP Material

Element	Cu	Al	Ni	Fe	Mn	Si	Pb
Min-Max	(min)79.0	8.5-9.5	4.0-5.0	3.5-4.5	0.8-1.5	0.10(max)	0.03(max)
Nominal	81	9	5	4	1	-	-
Alloy 1	81	9.39	4.29	3.67	1.20	0.05	<0.005
Alloy 2	81.2	<u>9.80</u>	4.71	<u>4.95</u>	1.01	0.08	0.01
740	80.30	9.44	4.86	3.90	1.25	0.04	0.01
741	81.07	9.27	4.67	<u>3.37</u>	1.35	0.04	0.01
751	80.68	9.31	4.76	3.69	1.30	0.04	0.01
754	80.16	9.38	4.66	4.41	1.20	0.05	<0.005
858-9	81.03	9.27	4.62	<u>3.45</u>	1.40	0.06	0.01

Table 1. Composition (wt.%) of UNS C95800 NAB (Adapted from [17])

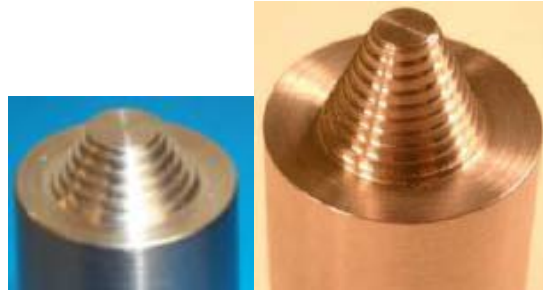


Figure 12. 6mm and 13mm FSP tools (From [13])

<b>FSP</b>	<b>Tool Size</b>	<b>Type</b>	<b>Pass</b>	<b>RPM/IPM</b>
740	6mm	Raster	Single Adv/Adv- Ret/Ret	Pass 1: 1000 / 4
741	6mm	Raster	Double Adv/Adv- Ret/Ret	Pass 1: 1000 / 4 Pass 2: 1000 / 4
751	6mm	Raster	Double Adv/Adv- Ret/Ret	Pass 1: 1000 / 4 Pass 2: 1000 / 10
754	13mm	Raster	Single Adv/Adv- Ret/Ret	Pass 1: 1000 / 4
858	13mm	Linear	Single	Pass 1: 1000 / 4
859	6mm	Linear	Single	Pass 1: 1000 / 4

Table 2. FSP process histories (See Figure 4a for multi-pass illustration)

## C. MICROSCOPY

### 1. Sample Preparation

Sample sections from were prepared using a Charmilles Andrew EF630 electric discharge machine (EDM) using consumable brass cutting wire with a nominal diameter of 0.10 mm. Sections were mounted in 1.25 inch premold - red phenolic using a Buehler SIMPLIMET 2 mounting press. Sample sections were mounted using an orientation axis so that the plane normal to the tool travel direction was viewable for all analysis and testing. Mounted samples were then mechanically polished following the schedule outlined in Table 3 for the indicated conditions using both Buehler ECOMET 4 and ECOMET 3 polishing wheels combined with the Buehler AUTOMET 2 powerhead.

After polishing steps 6 – 9 the samples were ultrasonically cleaned in methanol. Samples were etched for 1 second in an etching solution of 40ml water, 40ml ammonium hydroxide and 2ml hydrogen peroxide and then rinsed in water. They were then etched for 2 seconds in an etching solution of 60ml water, 30ml phosphoric acid and 10ml hydrogen peroxide and rinsed again.

Step	Abrasive	Time	RPM	Force
1	320 Grit SiC Paper	10 min.	150	5 lbs
2	500 Grit SiC Paper	10 min.	150	5 lbs
3	800 Grit SiC Paper	5 min.	150	5 lbs
4	1000 Grit SiC Paper	5 min.	150	5 lbs
5	2400 Grit SiC Paper	5 min.	150	5 lbs
6	4000 Grit SiC Paper	5 min.	150	5 lbs
7	3 micron Metadi Diamond Suspension	5 min.	90	2 lbs
8	1 micron Metadi Diamond Suspension	5 min.	90	2 lbs
9	0.05 micron Colloidal Silica	5 min.	90	2 lbs

Table 3. Mechanical Polishing Schedule (From [16])

## 2. Optical Microscopy

Optical microscopy was conducted using the Carl Zeiss JENAPHOT 2000, reflected light photomicroscope, with output via a PULNIX TMC-74 – CCD Camera. The digital output was used with SEMICAPS photo capturing and measurement software. Micrographs were prepared for montages of all FSP runs at 48X magnification. Micrographs of selected local microstructures were prepared at 370X magnification.

## D. TENSILE SAMPLING

### 1. Sample Preparation

Tensile samples were also sectioned using a Charmilles Andrew EF630 electric discharge machine (EDM) using consumable brass cutting wire with a nominal diameter of 0.10 mm. The advantage of using the EDM over diamond wafering or abrasive cutting is the ability for the machine to cut the complex geometries without imparting large external forces or excessive heat which may alter the material condition. The EDM also minimizes the amount of waste material. This allowed us to maximize the amount of test material from the available usable volume. The ability to tightly control the cutting lines also helped to increase confidence in our tensile testing results.

Each blank was cut individually and numbered prior to sectioning. Each tensile sample was numbered and indexed as it was sectioned from its respective blank. After machining, each tensile sample was hand surfaced by sanding all surfaces with 320 grit grinding wheels and emery paper. Particular care was taken to not allow heating due to friction.

## **2. Tensile Testing**

The computer controlled INSTRON Model 4507 with GPIB interface control and the Series IX data collection software was used to perform all tensile testing. Using a standard tensile test method with a constant cross head displacement speed the specimens were loaded to failure. Great care was exercised to properly align all samples as they were mounted into the screw platen type grips. A jig assembly, shown in Figure 13, was fabricated to ensure consistent sample alignment. A universal joint was also added between the load cell and the upper grip to aid in tensile load alignment. Prior to each test the load cell and extension length were reset, balanced and calibrated at the INSTRON control panel. During each run engineering stress, engineering strain, load cell and crosshead displacement data were gathered at 5 Hz and recorded in an ASCII 2 formatted file. Data were then imported into a locally prepared MATLAB m-file using MATLAB Version 6.5 for an analysis that compensated for the elastic response of the machine frame and grip. This was necessary because the min-samples were too small to fit with an extensometer.

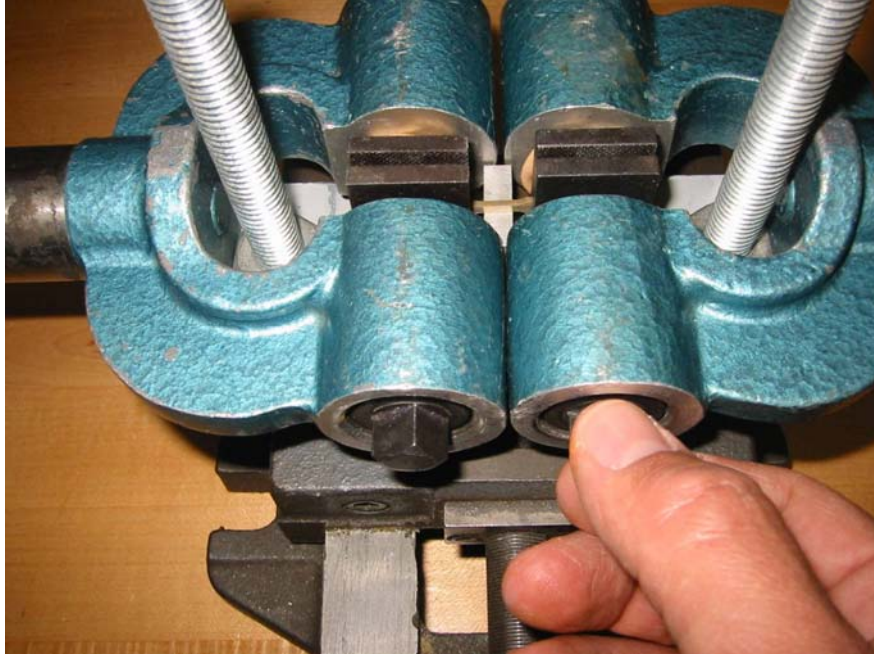


Figure 13. Aligning mini sample in grips

### **III. RESULTS AND DISCUSSION**

#### **A. TENSILE TEST DATA**

The ratio of the gage length to width for the tensile samples of this research (2.85:1) falls below that of Reference 18 (4.0:1). This reflected the need for a small sample for irregular, rolled materials (16) as well as to conserve material in the current study. Although yield and ultimate strengths should be independent of specimen size, ductility is specimen geometry dependent [18]. Because these samples generally exhibited little necking, it is anticipated that the specimen geometry will have little impact on ductility as well. Furthermore, the same geometry was used for all of this work so the data are internally consistent.

All materials were tested in accordance with section III. The results of mechanical property testing will be presented and the data then will be correlated with microstructure. All FSP material displayed a significant increase in yield and ultimate tensile strengths; however, in isolated cases slight ductility decreases were noted. In general, the best overall mechanical and microstructural properties were found down the apparent center of an FSP bead.

Due to an error in machining of the tensile samples for FSPs 858 and 859, the samples representing the greatest depth, (samples numbered 8), were not testable. Samples 1-7 provide coverage of the stir zone but do not provide the transition to base metal for the very bottom of the TMAZ in FSP 858.

Figure 14 shows a representative example of the tensile data for the 3-series of FSP 754. Tabular results for all tensile tests were compiled into Tables 4 and 5. The data generated from plotting these plots in MATLAB was used to generate the contour and mesh plots such as those in Figures 15-17.

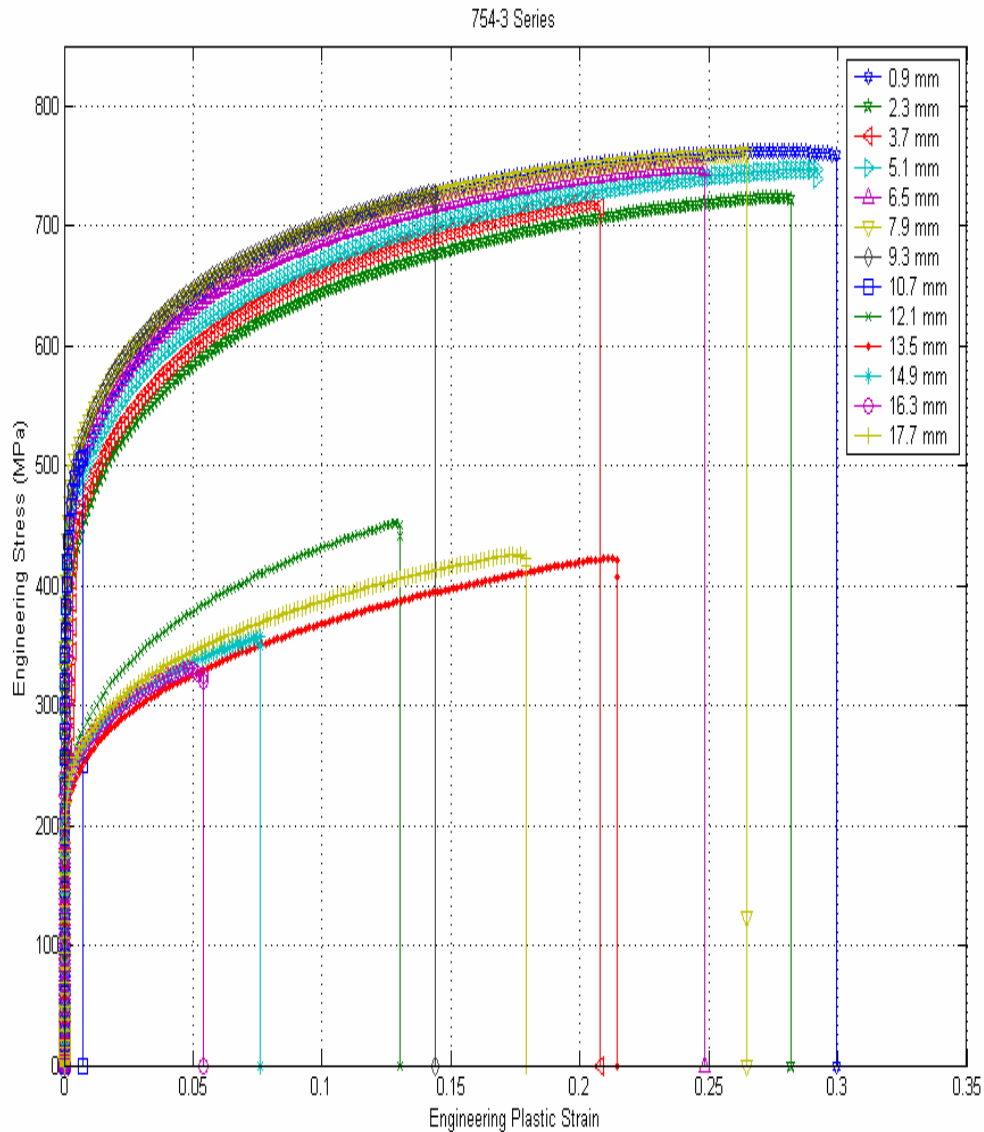


Figure 14. Typical stress strain plots; the depth below the surface is indicated for each sample.

Figure 14 illustrates the significant increase in ductility and the doubling in both yield and ultimate tensile strengths in the first seven (upper) samples. These samples were all within the stir zone for FSP 754. There is also a drastic decrease in ductility at a depth of 10.7mm. As depth increases, the samples represent the TMAZ and HAZ regions and then, eventually, the base metal. For depths between 10.7mm and 12.1mm, the

samples are in regions corresponding to the TMAZ or HAZ (there is some upward displacement of the tool). At a depth of 17.1mm, the sample lies in base metal.

	NAB Base Metal			FSP 858 (13mm tool)			FSP 859 (6mm tool)		
	Yield	UTS	EP	Yield	UTS	EP	Yield	UTS	EP
<b>Blank 1</b>				<b>Retreating Side</b>			<b>Retreating Side</b>		
1	226.61	349.94	0.18	363.52	415.00	0.04	548.25	702.76	0.09
2	242.28	299.07	0.07	278.39	322.72	0.06	485.18	500.11	0.02
3	201.62	206.18	0.03	265.65	321.03	0.06	456.66	578.00	0.10
4	224.57	370.43	0.18	268.42	369.74	0.11	316.62	461.64	0.13
5	161.31	169.60	0.01	251.61	347.71	0.12	238.92	366.69	0.19
6	243.05	390.92	0.20	260.70	369.82	0.13	227.19	384.05	0.30
7	233.80	348.77	0.16	272.40	417.41	0.20	213.52	215.82	0.02
<b>Blank 2</b>				<b>Retreating Side</b>			<b>Center Line</b>		
1	200.21	291.05	0.15	549.47	715.04	0.14	546.63	777.86	0.19
2	216.19	286.26	0.11	510.38	677.97	0.11	516.72	702.93	0.14
3	203.97	335.46	0.20	474.80	496.25	0.04	517.19	713.67	0.15
4	223.80	383.18	0.22	523.77	613.44	0.06	513.46	701.76	0.13
5	215.58	222.66	0.00	479.90	564.32	0.06	484.50	616.21	0.08
6	217.31	242.65	0.04	438.65	556.13	0.09	266.79	383.65	0.15
7				325.84	469.49	0.14	254.50	312.78	0.07
<b>Blank 3</b>				<b>Center Line</b>			<b>Advancing Side</b>		
1	188.83	208.66	0.00	535.29	750.55	0.18	550.09	774.58	0.20
2	248.58	330.71	0.10	482.05	701.54	0.16	512.01	726.72	0.21
3	248.84	330.42	0.11	495.74	715.50	0.21	505.33	673.74	0.14
4	205.26	204.28	0.02	549.42	763.97	0.19	412.84	604.52	0.21
5	240.41	310.38	0.10	536.80	746.24	0.19	235.59	358.56	0.20
6	227.88	246.77	0.05	539.05	706.07	0.12	202.24	211.47	0.03
7	238.26	286.01	0.07	536.01	713.49	0.14	198.75	198.75	0.02
<b>Blank 4</b>				<b>Advancing Side</b>					
1	234.15	373.73	0.23	547.95	768.57	0.19			
2	235.74	242.79	0.03	543.41	719.72	0.13			
3	240.27	283.02	0.08	503.99	674.65	0.13			
4	229.65	337.91	0.19	425.24	513.82	0.07			
5	238.93	305.46	0.10	444.38	554.87	0.08			
6	194.84	280.78	0.12	401.33	520.10	0.09			
7	227.12	397.30	0.31	317.63	428.46	0.10			
<b>Blank 5</b>				<b>Advancing Side</b>					
1				410.43	537.56	0.08			
2				292.74	288.18	0.02			
3				296.54	399.02	0.13			
4				254.21	257.13	0.00			
5				291.60	306.73	0.04			
6				301.12	412.97	0.16			
7				308.49	395.56	0.12			

Table 4. FSP Yield and Ultimate Tensile Strengths, with Elongation (Base Metal, 858 & 859)

	754 (13mm tool)				740 (6mm tool)				741 (6mm tool)				751 (6mm tool)			
	Yield	UTS	EP		Yield	UTS	EP		Yield	UTS	EP		Yield	UTS	EP	
<b>Blank 1</b>	<b>Retreating Side</b>				<b>Retreating Side</b>				<b>Retreating Side</b>				<b>Retreating Side</b>			
1	580.92	767.27	0.26		611.63	751.04	0.11		598.13	782.74	0.22		646.46	809.70	0.27	
2	532.41	746.62	0.30		573.02	775.27	0.23		527.66	747.96	0.33		581.28	783.64	0.20	
3	532.97	709.35	0.20		589.13	781.35	0.24		538.96	758.91	0.28		595.99	802.62	0.22	
4	544.41	731.92	0.21		549.84	654.92	0.11		553.16	763.97	0.26		638.61	832.17	0.21	
5	564.72	735.61	0.23		570.34	754.97	0.22		570.03	726.81	0.25		649.05	811.64	0.23	
6	587.57	762.99	0.25													
7	534.49	546.04	0.01													
8	484.25	571.65	0.07													
9	302.17	329.21	0.04													
10	289.57	345.82	0.07													
11	293.88	362.34	0.08													
12	288.89	351.68	0.08													
13	260.31	290.20	0.04													
<b>Blank 2</b>	<b>Center Line</b>				<b>Center Line</b>				<b>Center Line</b>				<b>Center Line</b>			
1	554.76	764.73	0.28		562.73	773.05	0.31		588.10	768.53	0.25		603.99	822.87	0.19	
2	556.68	759.31	0.32		538.13	772.12	0.31		547.10	759.83	0.33		608.87	801.58	0.17	
3	563.64	755.40	0.33		553.44	774.10	0.30		513.08	732.74	0.21		535.15	773.40	0.18	
4	563.59	776.76	0.28		582.11	783.48	0.28		559.93	768.06	0.31		607.47	773.36	0.15	
5	553.54	745.41	0.22		534.79	703.92	0.17		575.10	698.86	0.11		636.05	775.60	0.15	
6	555.47	747.29	0.24													
7	555.31	746.60	0.22													
8	577.54	751.90	0.22													
9	345.98	367.81	0.03													
10	292.81	406.29	0.16													
11	309.00	354.63	0.06													
12	319.31	389.68	0.09													
13	287.63	426.81	0.18													
<b>Blank 3</b>	<b>Advancing Side</b>				<b>Advancing Side</b>				<b>Advancing Side</b>				<b>Advancing Side</b>			
1	556.94	758.87	0.30		575.37	787.10	0.24		600.90	725.82	0.09		589.38	808.84	0.29	
2	507.89	722.12	0.28		520.60	746.97	0.23		563.90	780.46	0.31		564.47	791.17	0.30	
3	520.65	715.97	0.21		555.58	645.20	0.06		584.57	777.70	0.28		574.74	802.75	0.31	
4	538.83	746.48	0.29		591.65	750.60	0.15		592.26	776.34	0.25		586.59	781.15	0.25	
5	558.60	746.17	0.25		560.64	733.97	0.24		553.88	759.03	0.28		600.07	764.98	0.18	
6	571.77	759.50	0.26													
7	574.82	727.45	0.14													
8	506.40	506.40	0.01													
9	319.98	450.75	0.13													
10	280.76	421.37	0.21													
11	293.57	357.10	0.08													
12	293.75	324.61	0.05													
13	297.83	423.35	0.18													

Table 5. Yield and Ultimate Tensile Strengths, with Elongation (754, 740, 741, & 751)

Altogether, 27 tests were conducted on samples from the unaffected base metal. These data give average values as follows: Yield Strength = 222.56 +/- 20.79; Ultimate Tensile Strength = 297.57 +/- 63.33; and ductility = 0.11 +/- 0.08. The large standard deviation for the ductility data likely reflects the small tensile sample size relative to defects such as porosity, in the material. Thus some low ductility samples had defects of size comparable to the samples minimum dimension. Examination of Tables 4 and 5

shows that single-pass FSP (FSPs 858 & 859) produces a significant increase in ductility with an increase from 10 to approximately 20 percent in elongation. Of even particular note is the increase from 10 to approximately 30 percent elongation in the multi-pass rastered FSP materials.

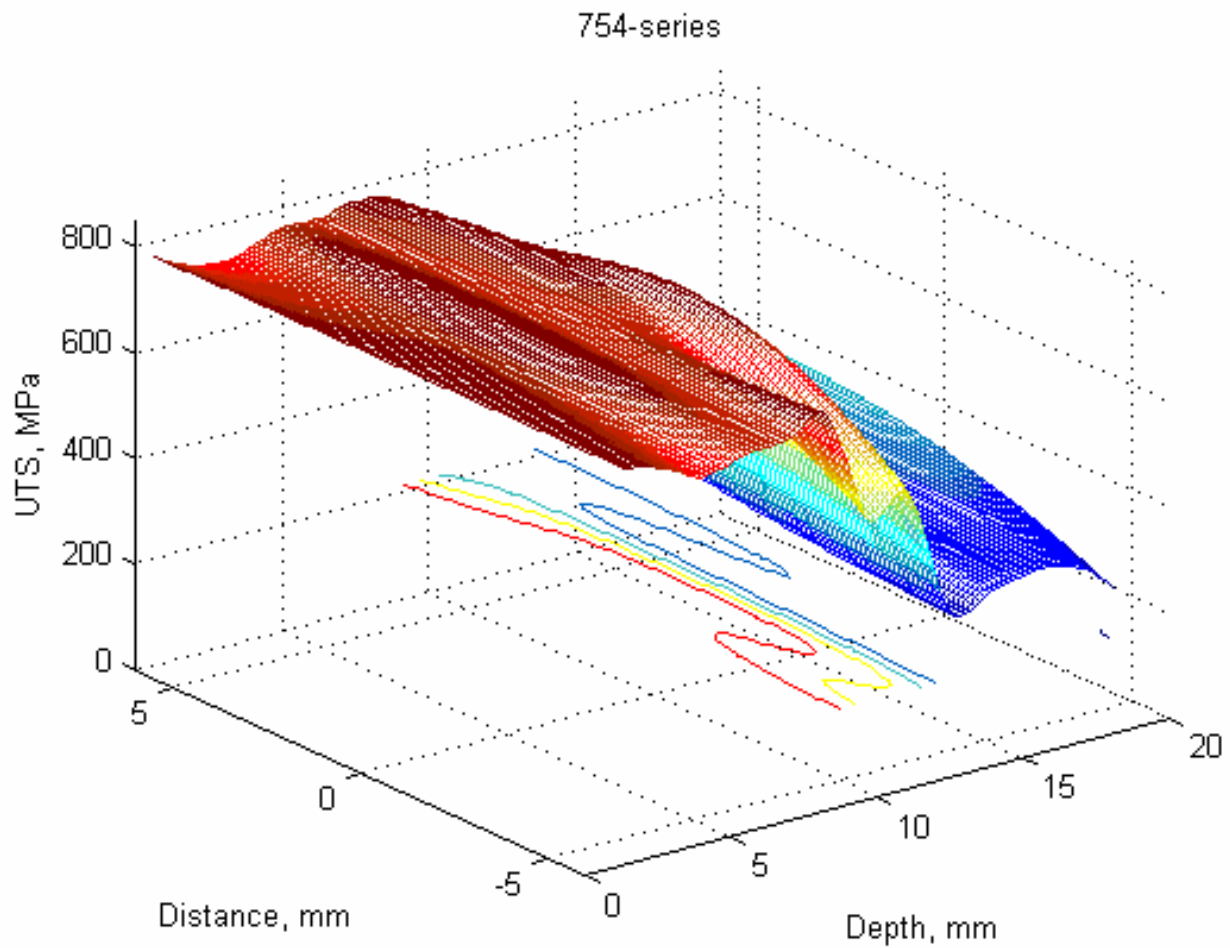


Figure 15. FSP 754 UTS mesh plot

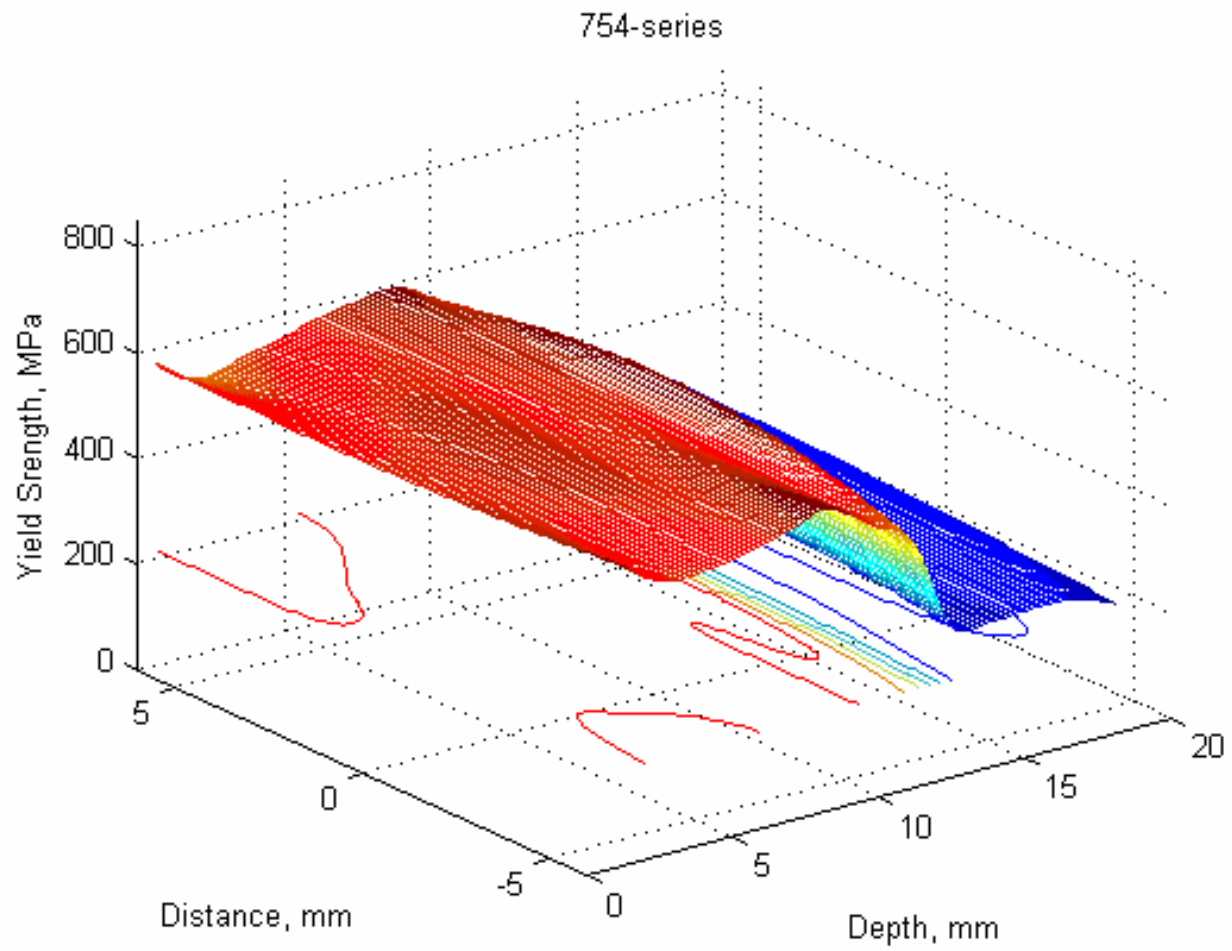


Figure 16. FSP 754 yield strength plot

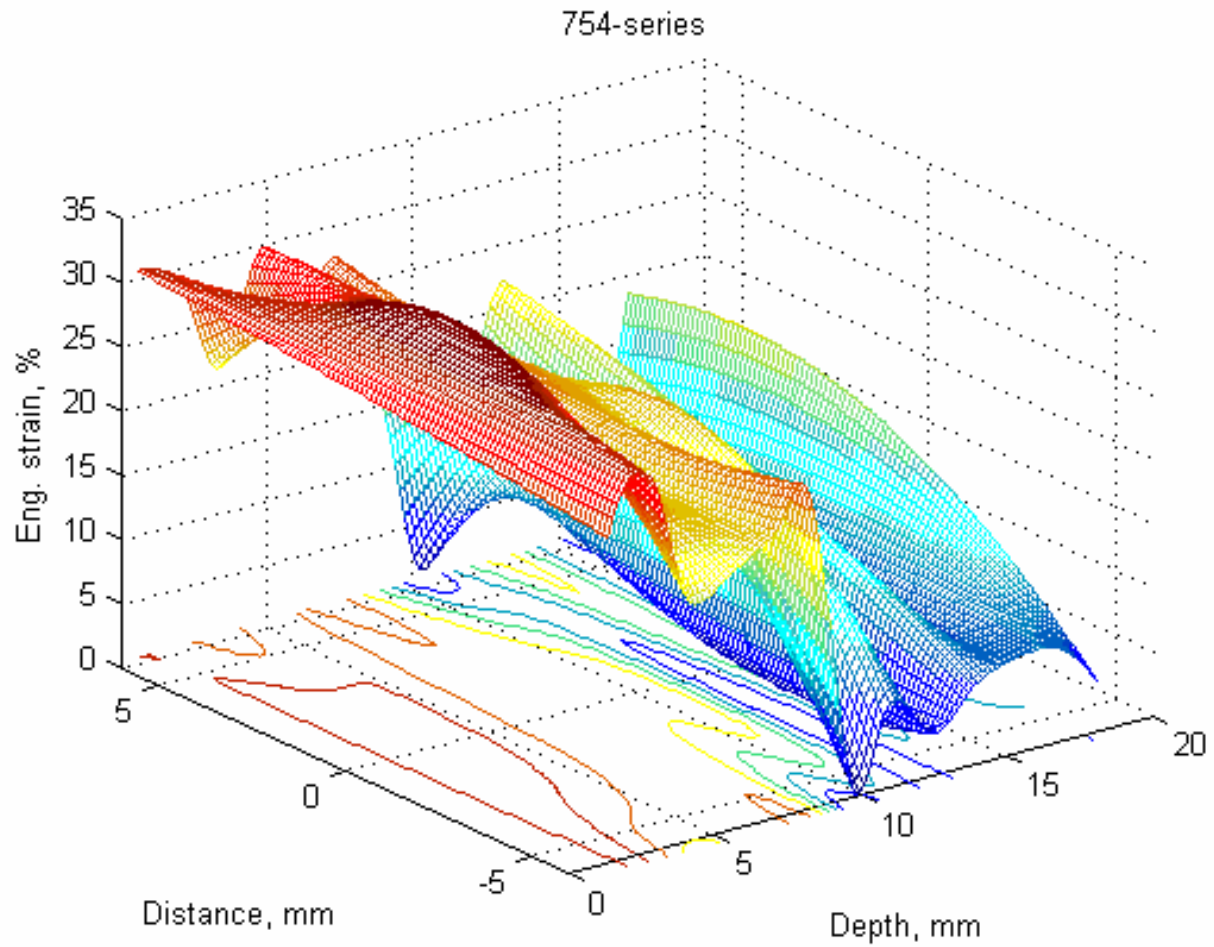


Figure 17. FSP 754 ductility plot

From Figures 15 – 17, it is notable that while both ultimate and yield strengths both steadily rise in the HAZ and TMAZ, located between 10mm and 15mm depth, the ductility is reduced below that of base metal in these areas and does not increase until a the depth is less than 10mm.

## B. MICROSTRUCTURE PROPERTY CORRELATIONS

### 1. Areas of High Ductility

Areas of highest ductility were normally found in the upper portion of the apparent nugget center. Microstructures most often associated with high ductility were either Widmanstätten or fine homogenous equiaxed grains. Figures 18 and 19 are examples of high ductility areas and microstructures. It is notable that the maximum ductilities observed in the linear, single-pass runs were about 20% while in the raster pattern runs of either single or double pass, ductilities of greater than 30% were observed.

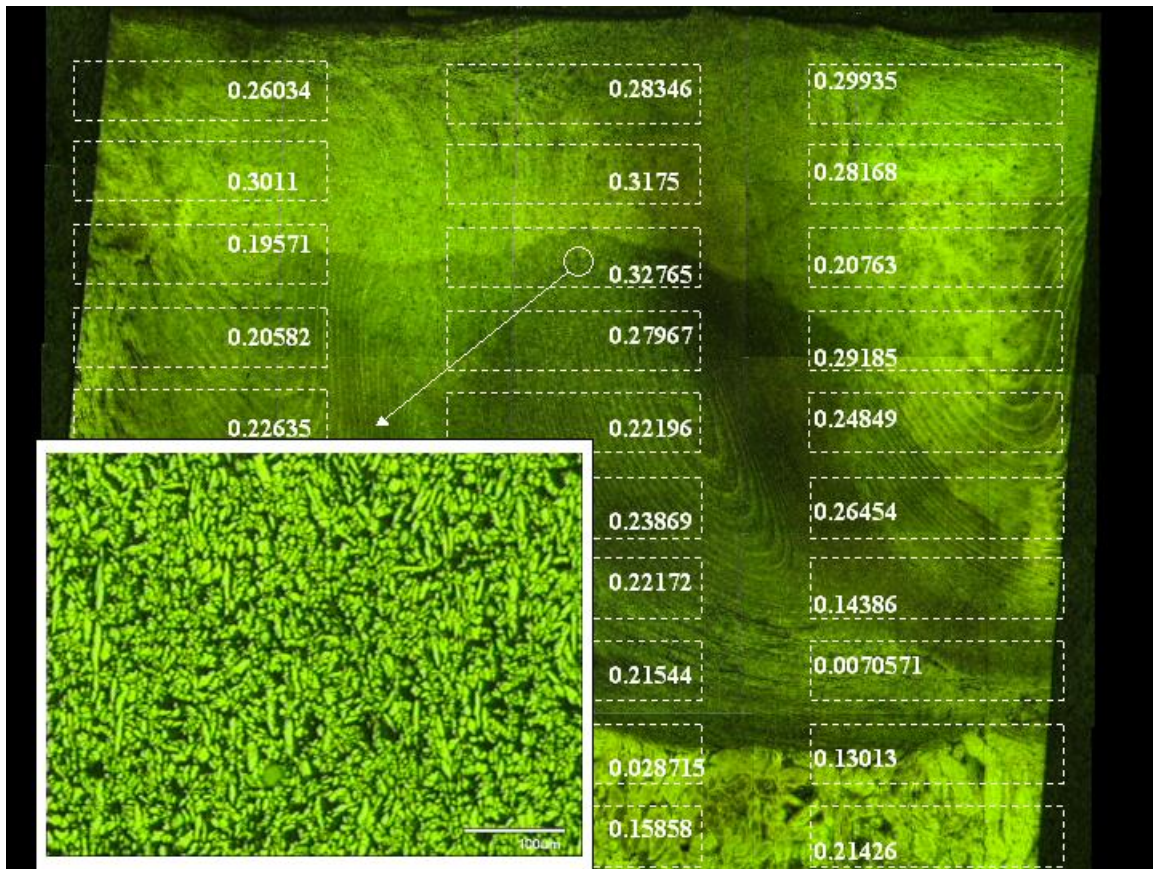


Figure 18. Area of highest ductility in FSP 754 and its microstructure. Local ductilities are indicated within the grid end outline that shows individual tensile sample locations.

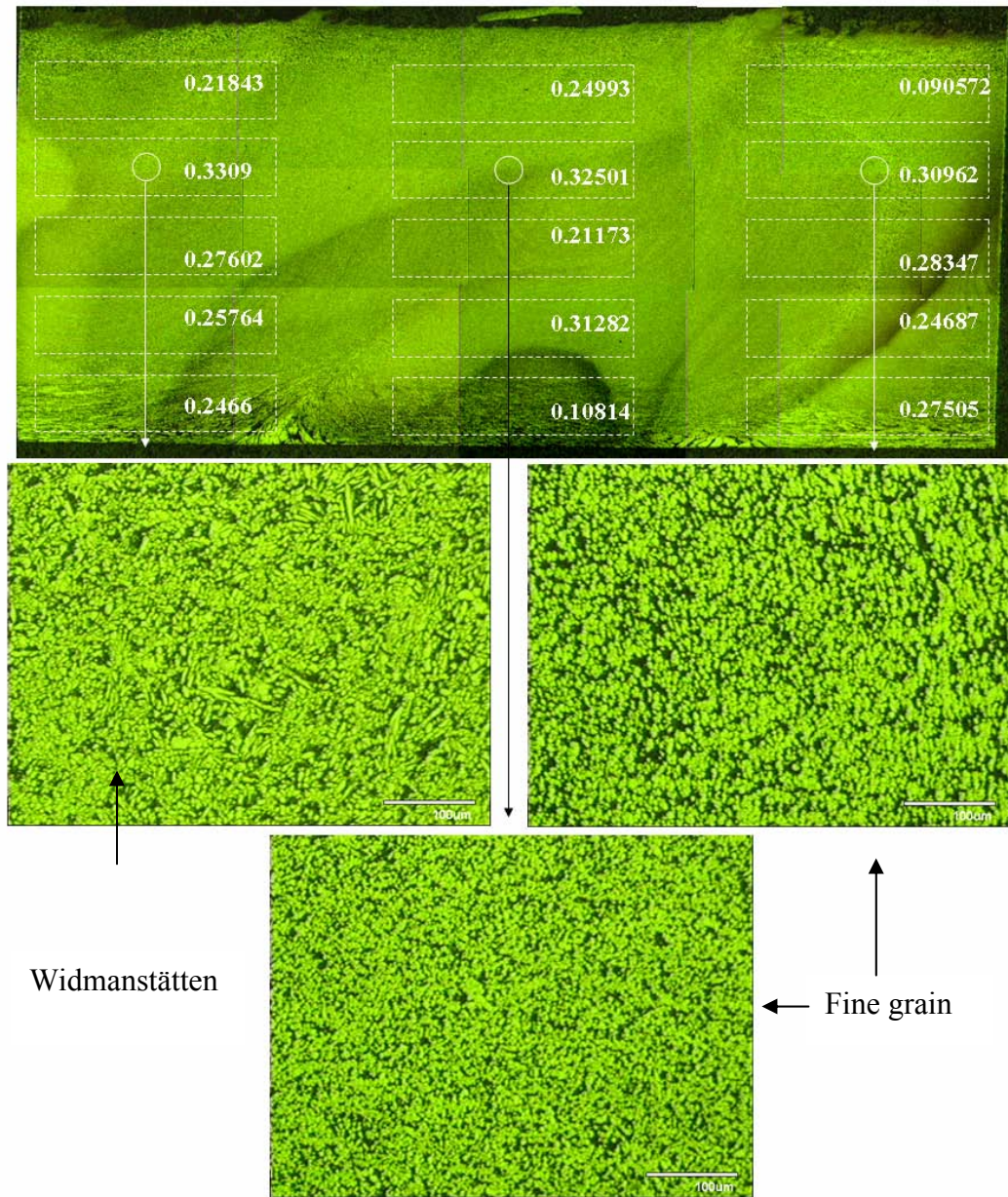


Figure 19. Areas of high ductility and associated microstructures from FSP 741

## 2. Areas of Low Ductility

Areas of low ductility within the stir nugget were normally associated with directional or non-equiaxed microstructures. Low ductility areas were also noted at the stir zone interface where a composite microstructure exists within the TMAZ. Additionally, areas of low ductility were found just within the heat affected zone where the base metal was heated to the eutectoid region without being strained. The presence of

coarse  $\kappa_{ii}$  was noted in a number of low ductility areas processed with the 13mm tool. Figure 20 shows the location, microstructure and fractography of a typical low ductility area within the stir zone of a single pass raster process. Figures 21 and 21 display composite microstructures observed within the TMAZ. Figure 23 presents an example of heat affected, non-strained base metal and low ductility.

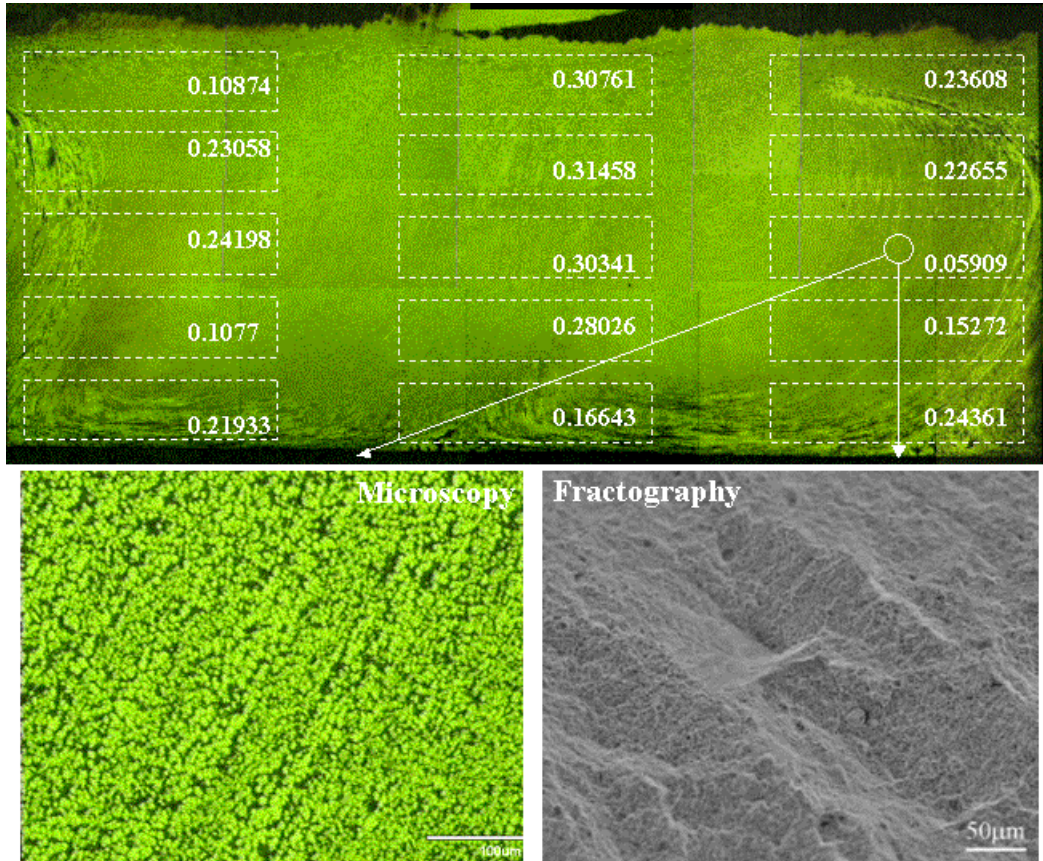


Figure 20. Montage, micrograph and fractography of FSP 740  
Local ductilities are indicated within the grip end outline that shows individual tensile sample location.

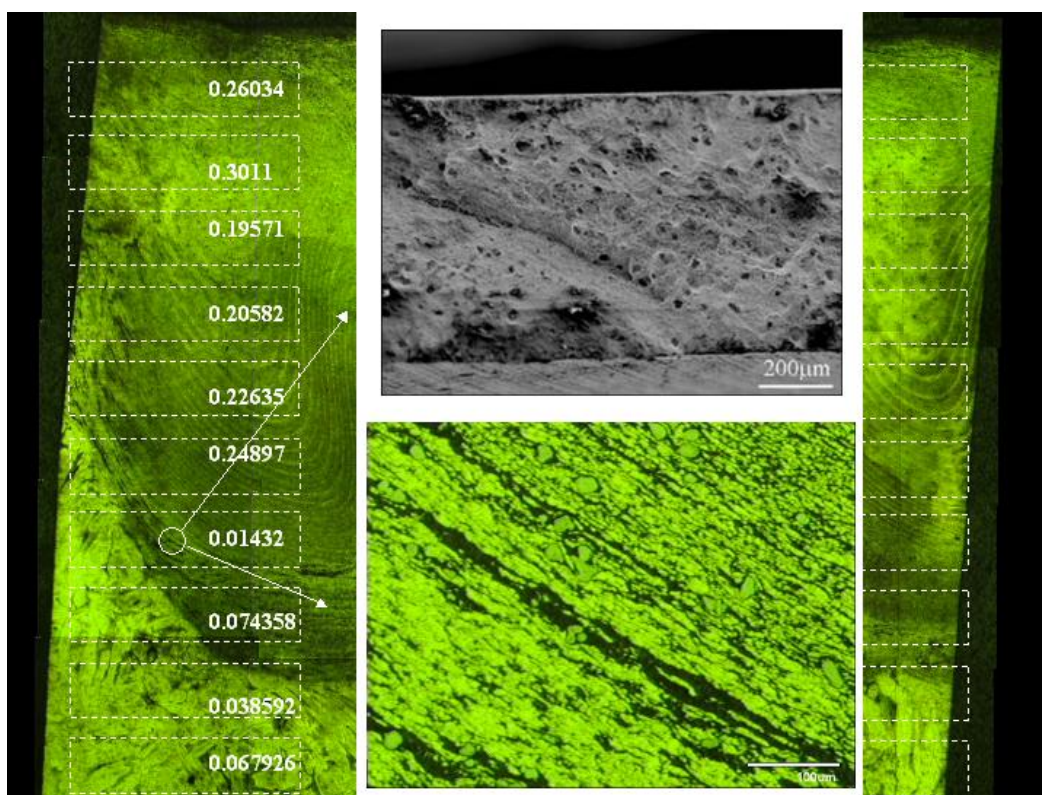


Figure 21. Montage, micrograph and fractography of FSP 754 (blank #1)

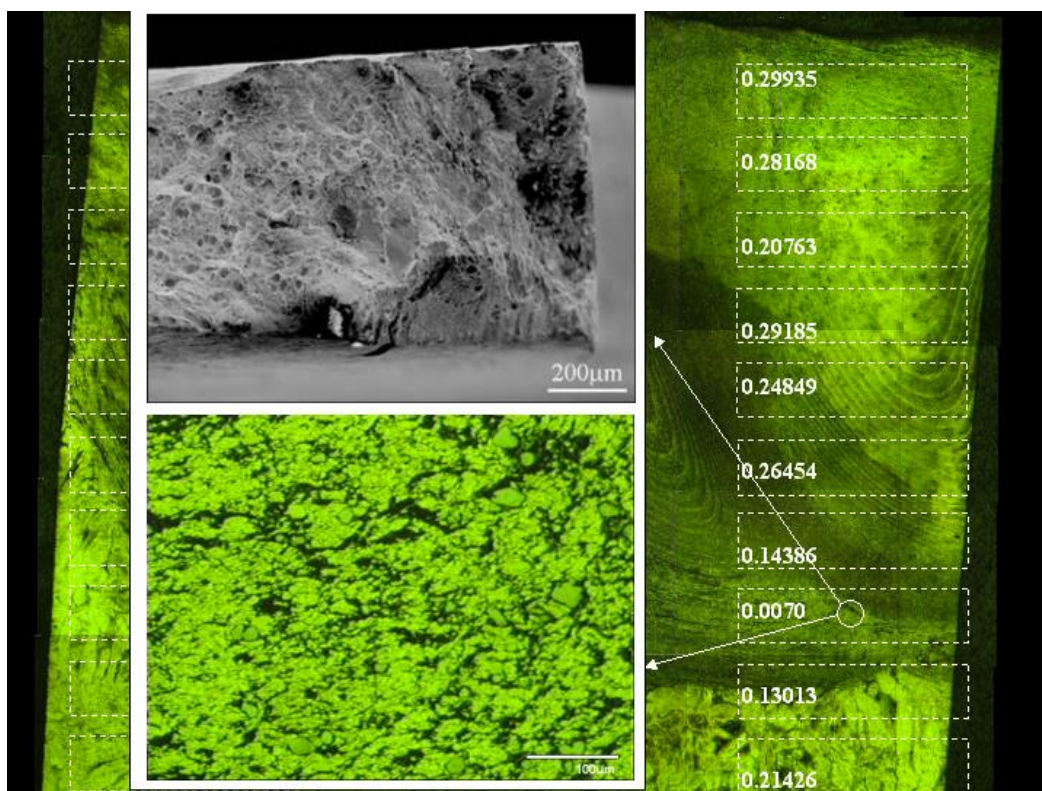


Figure 22. Montage, micrograph and fractography of FSP 754 (blank #3)

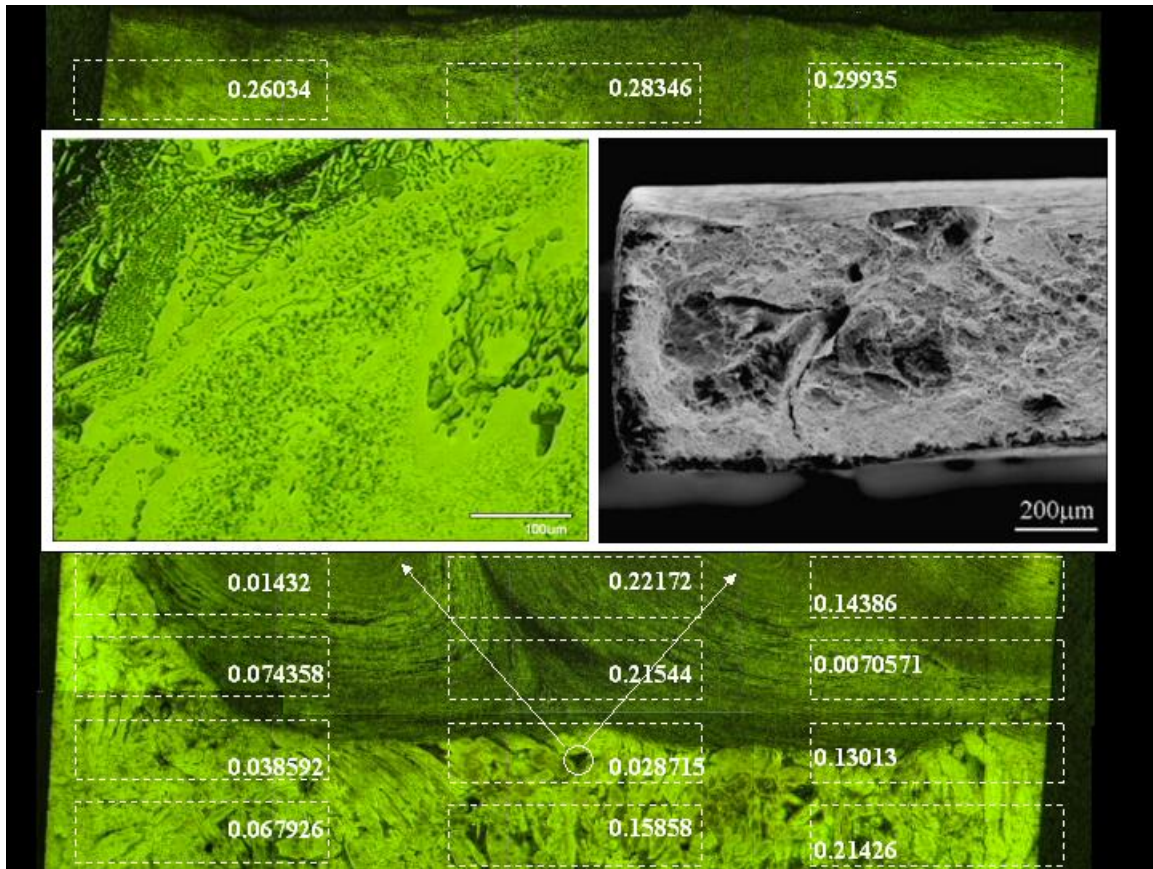


Figure 23. Montage, micrograph and fractography of FSP 754 (blank #2)

### 3. Ductility Contours

Contour and mesh plots, Figures 24-26, were generated from tensile test data and superimposed on micrograph montages. In FSP 859 and FSP 754, where a significant amount of base metal is not processed, the TMAZ and transition to HAZ areas appear to experience a significant decrease in ductility, while yield and ultimate tensile strengths remain slightly above that of unprocessed NAB.

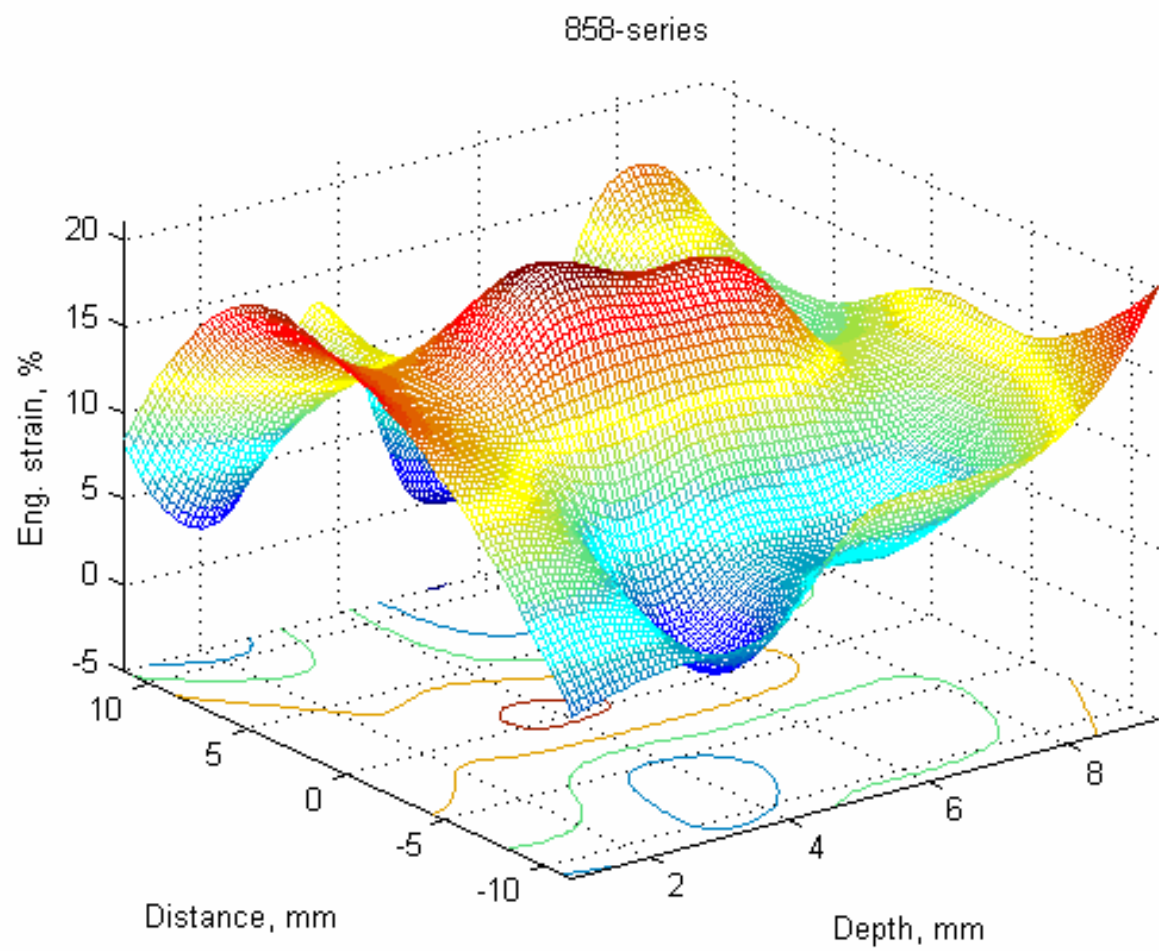


Figure 24. FSP 858 ductility mesh plot

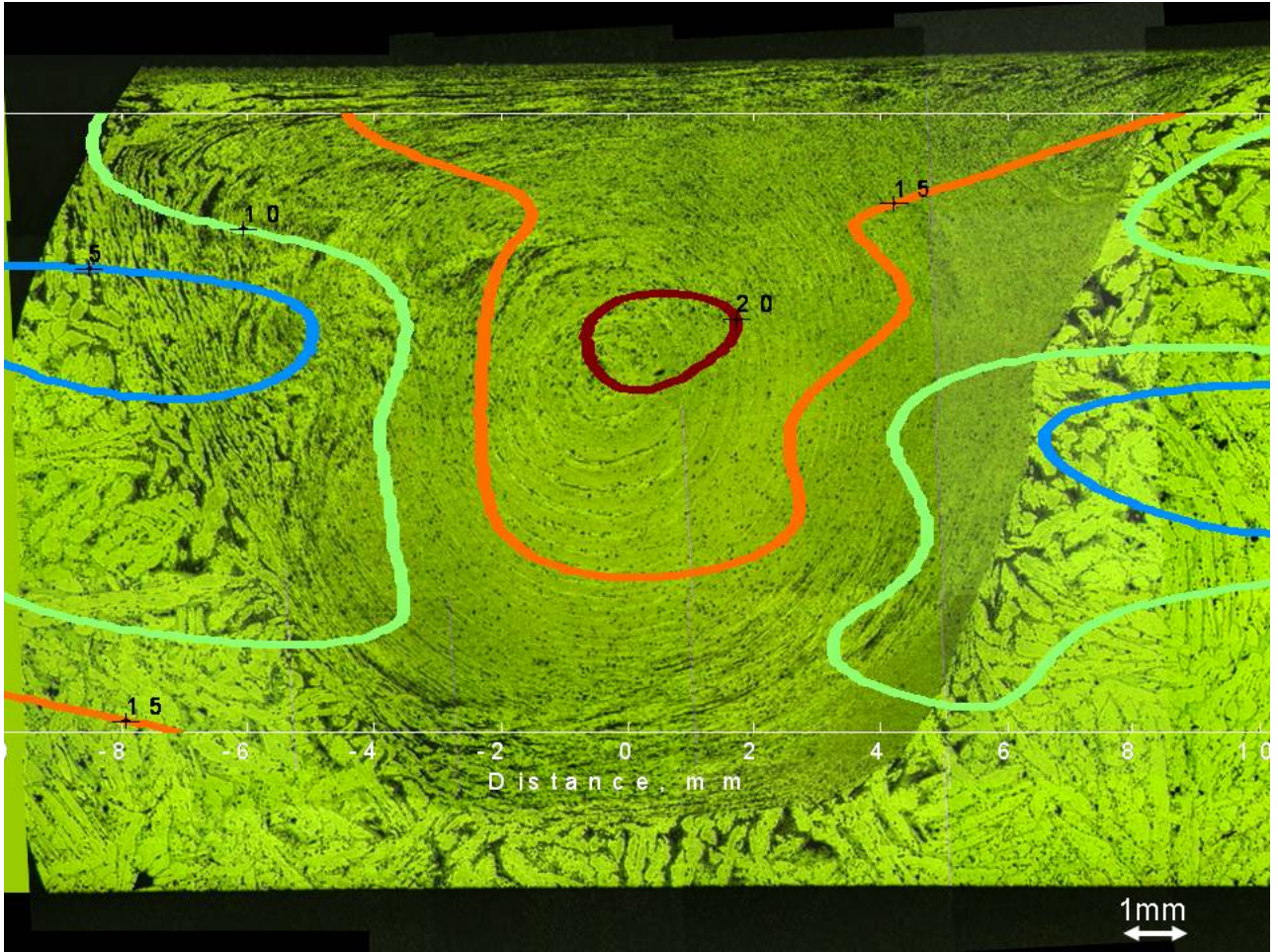


Figure 25. FSP 858 ductility contour plot

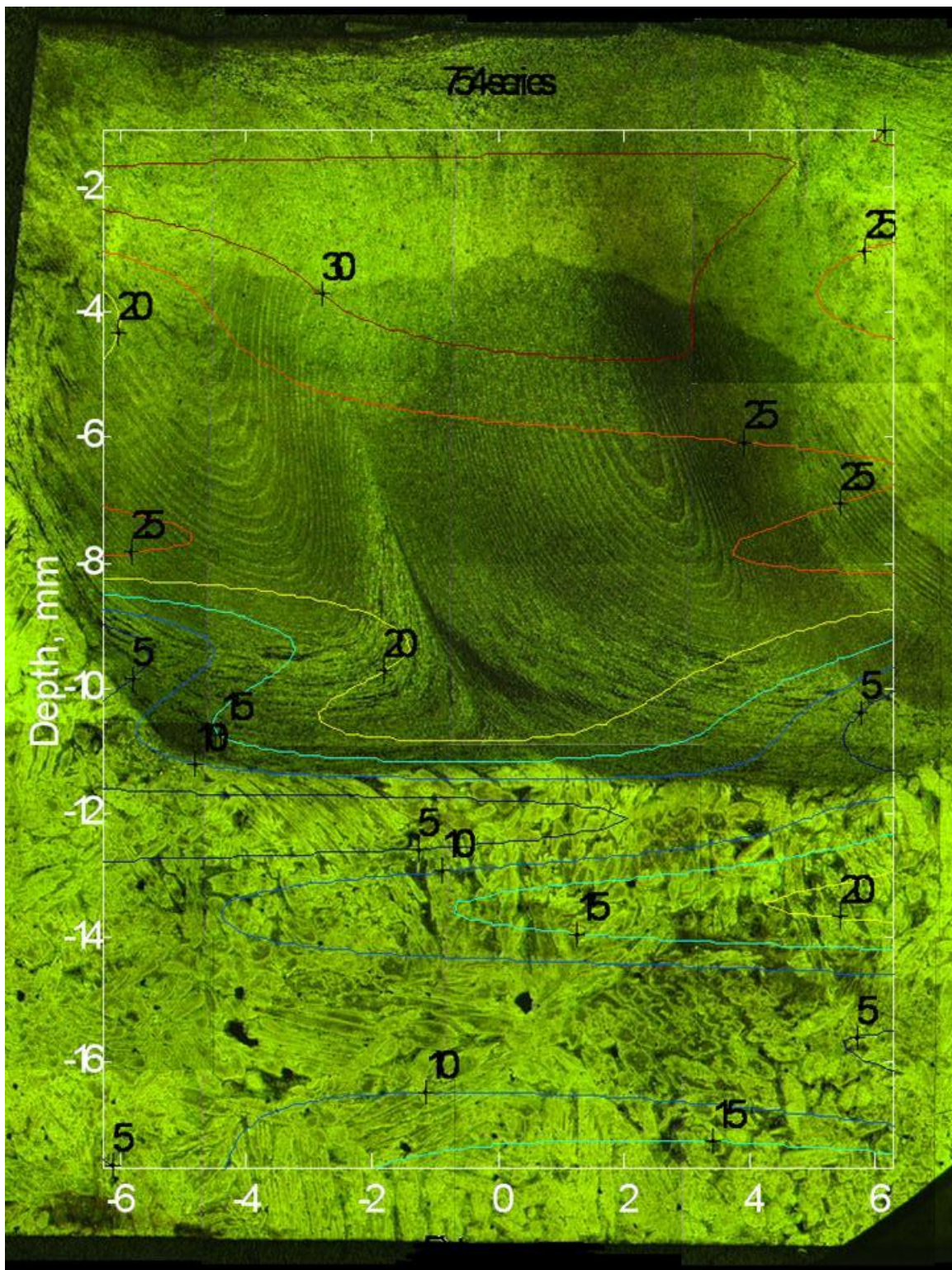


Figure 26. FSP 754 ductility contour plot

## C. CORRELATION OF DUCTILITY WITH MICROSTRUCTURE

### 1. High Ductility

Altogether, tensile ductilities of 20 percent to 30 percent elongation to failure were observed in stir zones along the centerline of the zone, i.e. along the direction of tool advance. Higher ductility in this range corresponded to multi-pass and raster pattern processes whereas the lower ductility values in the range were associated with single passes. This suggests that increased strains and additional thermomechanical cycles during FSP further refine microstructures and further reduce defects within the stir zone volume. The highest ductilities were observed in association with either fully Widmanstätten-type microstructures or fine, equiaxed  $\alpha$ . From ongoing work in this laboratory [19], these microstructures reflect local peak temperatures of  $>950^{\circ}\text{C}$  in the stir zone, such that a high volume fraction of  $\beta$  forms upon heating and then transforms during subsequent cooling. The high ductility of the resulting Widmanstätten-type or fine, equiaxed  $\alpha$  microstructures is consistent with Pierce's [16] data from hot rolling studies, wherein hot rolling to large strains at  $950^{\circ} - 1000^{\circ}\text{C}$  resulted in these same microstructure types and tensile elongations of up to 30 percent during tension testing. In single pass samples (858 and 859) ductility varied with location in stir zones and was typically lower on either side of the stir zone centerline. However, no systematic variation with respect to the advancing or retreating sides of the stir zone was noted. In multi-pass and rastered materials, ductility was more consistently high across the upper regions of the stir zone and ductility decrease with depth in the stir zone. Finally, infrequent low ductility values were observed within stir zone and may have been associated with distinct onion-ring type structures.

Within all of the stir zone of this study, both strength and ductility to improved due to FSP. This situation is very unique. Normally heat treatment will increase strength while ductility suffers. This is true for heat treatment only applied to NAB; e.g., see Pierce's data [16] and is also true of most heat treatable alloys. For FSP of NAB, this reflects the refining effect of the severe  $^{\circ}$ deformation on a coarse, as-cast material coupled with the refined and strong microstructures produce by phase transformation from the  $\beta$  produced during heating due to the processing.

## 2. Low Ductility

For the materials tested in this investigation, a significant drop in ductility was observed at the stir zone - TMAZ boundary, where there is an interface and composite microstructures in tensile samples, and just within the HAZ, where base metal is heated but not strained. Composite microstructures would comprise both highly refined stir zone structures, such as fine-grained, with material that has been heated only to temperatures near the eutectoid and then deformed relatively lightly. Again, Vazquez' [15] and Pierce's [16] data from hot rolling studies indicated that hot rolling to small strain at temperature of 800° - 900°C resulted in low tensile ductility in association with severely strained primary  $\alpha$ . Also, at such temperatures the  $\kappa_{ii}$  remains undissolved and coarse particles of this phase may contribute to low ductility. In samples having composite microstructures, one part of the sample would consist of a strong, ductile microstructure of the stir zone and the remainder would be weaker and less ductile material from the TMAZ. Under isostrain conditions for samples having axes parallel to tool traversing direction, the weaker portion could attain its fracture strength before the stronger portion reaches its yield strength. Thus the tensile behavior would be dominated by the properties of the lower strength portion. The reduced ductility from thermal cycling in the absence of strain (i.e., in the HAZ) is, again, consistent with previous studies and results of heat treatment as summarized in Figure 6 [15, 16]. The low ductility may not reflect FSP but rather only the thermal cycle of the process. On this basis, conventional arc welding, such as used in buttering and weld repair of defects, would likewise be expected to give a low ductility region in the corresponding HAZ. This will require further investigation using miniature samples such as those of the current investigation.

THIS PAGE INTENTIONALLY LEFT BLANK

## **IV. CONCLUSIONS AND RECOMMENDATIONS**

### **A. CONCLUSIONS**

1. The stir zone generally exhibits improved strength and ductility in comparison to base metal.
2. Multi-pass and raster processes generally give higher ductility and strength combinations than single-pass materials.
3. Low ductility values were sometimes observed in stir zones.
4. Low ductility generally coincided with mixed stir zone /TMAZ or HAZ microstructures.

### **B. RECOMMENDATIONS FOR FUTURE RESEARCH**

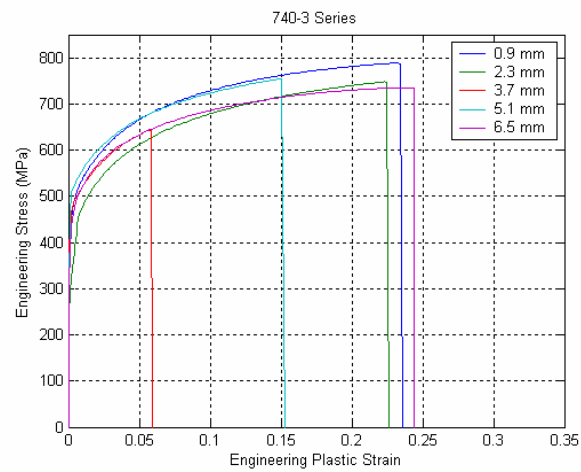
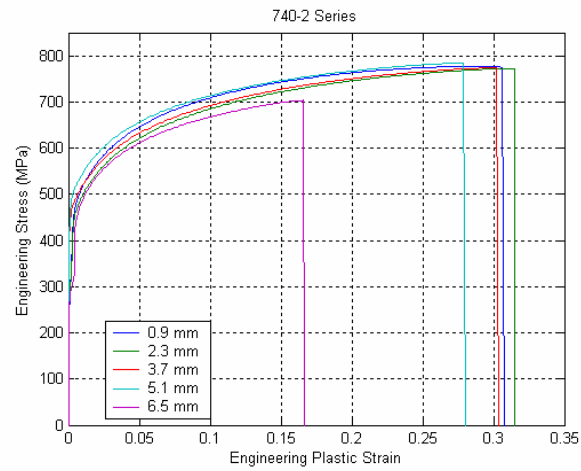
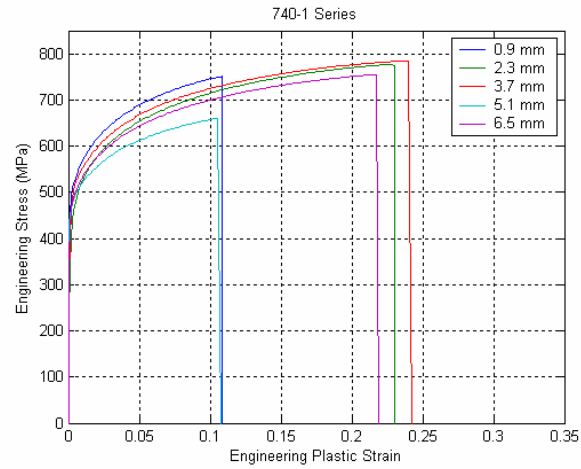
The following areas are recommended for further research:

1. Investigate the effect of active temperature controlled FSP on microstructure in the areas noted for low ductility.
2. Investigate the effects of various combinations of post-weld heat treatments on microstructure in the areas noted for low ductility in FSP material.
3. Investigate the HAZ of conventional weld repairs to determine if a similar reduction in ductility is present.

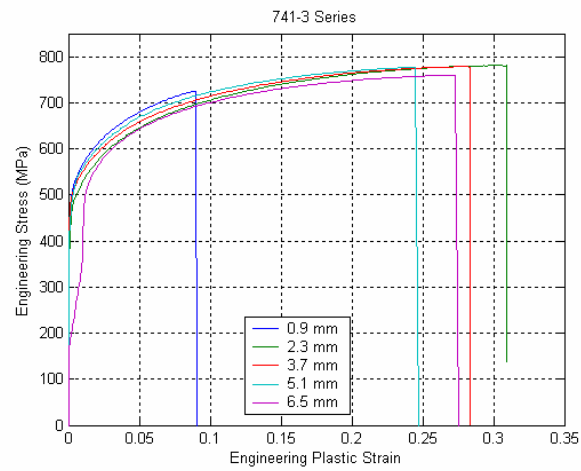
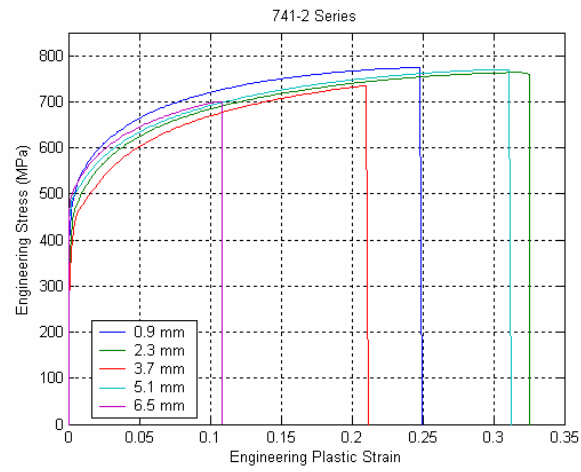
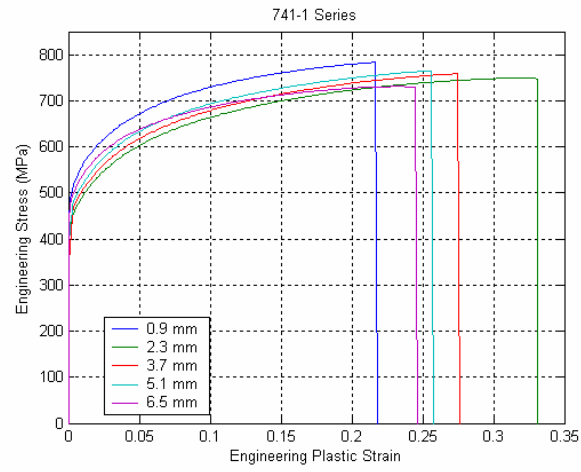
THIS PAGE INTENTIONALLY LEFT BLANK

## APPENDIX A – STRESS VS. STRAIN PLOTS

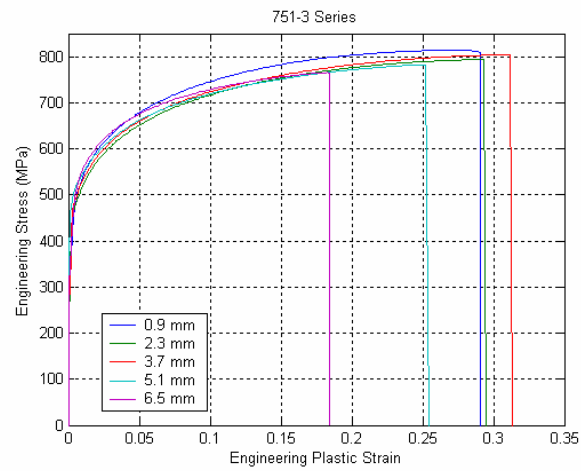
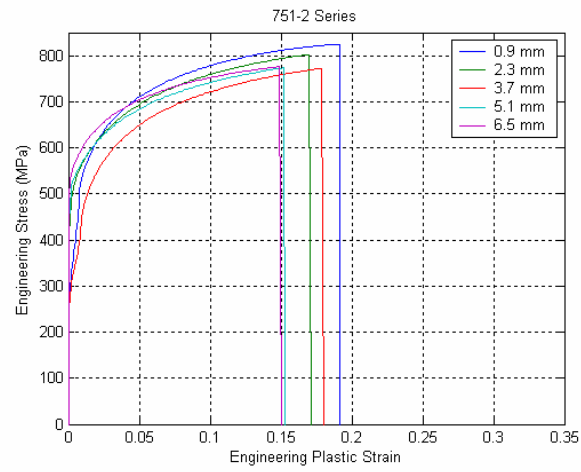
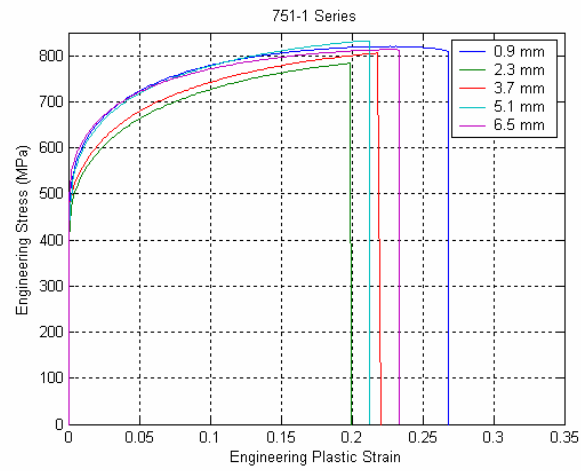
### A. 740 SERIES



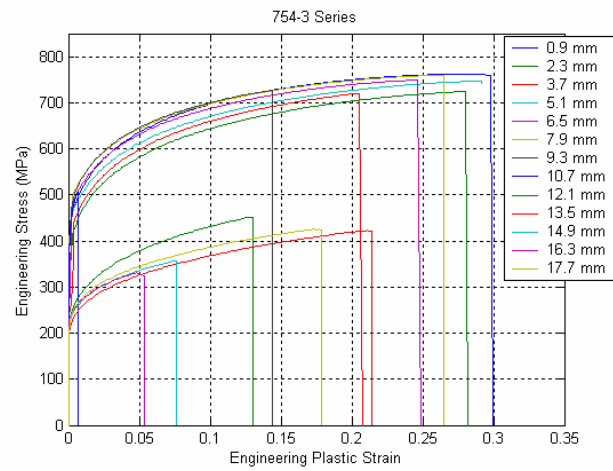
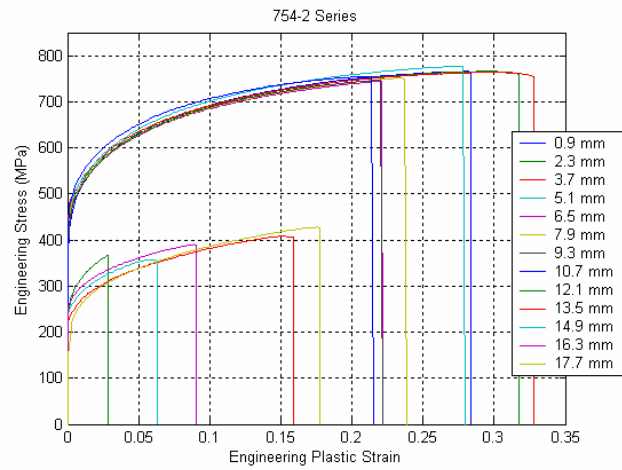
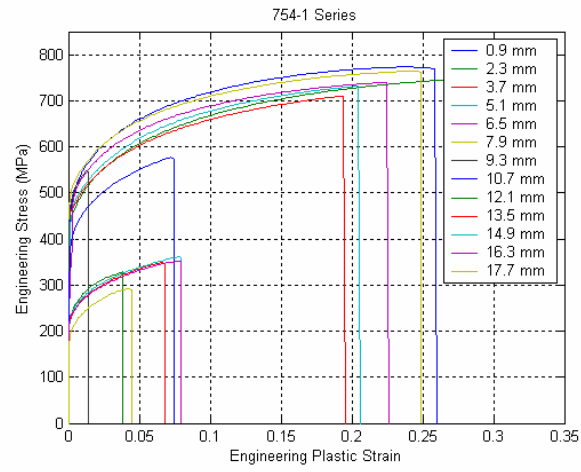
## B. 741 SERIES



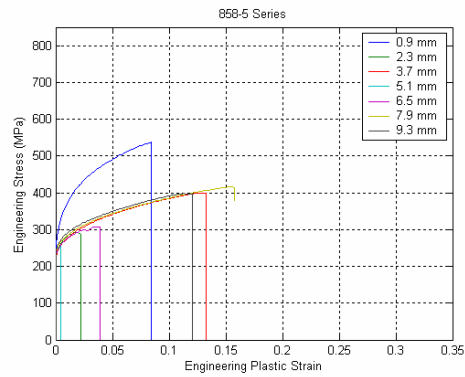
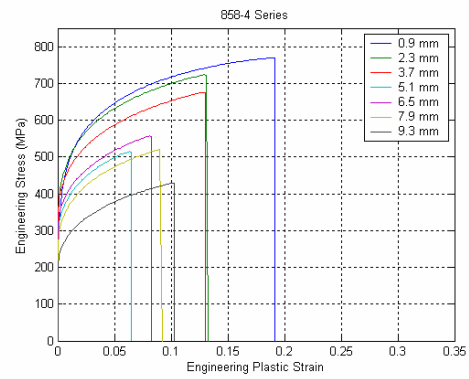
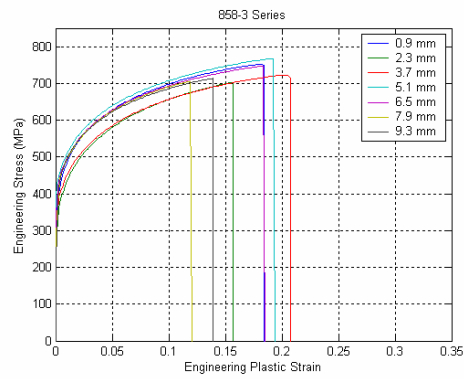
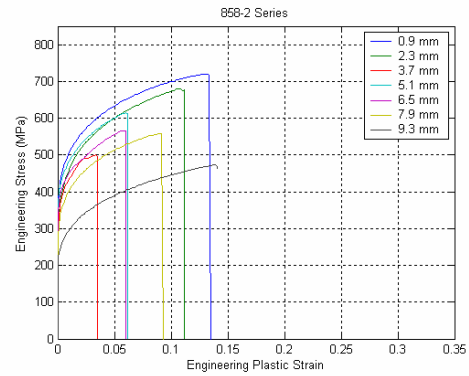
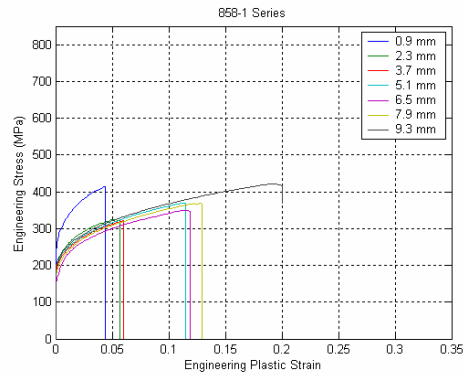
## C. 751 SERIES



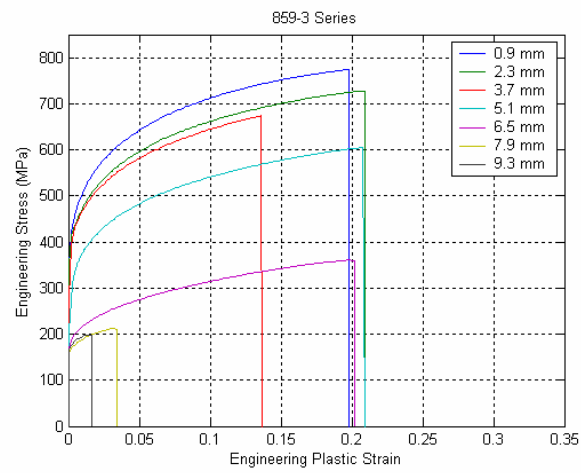
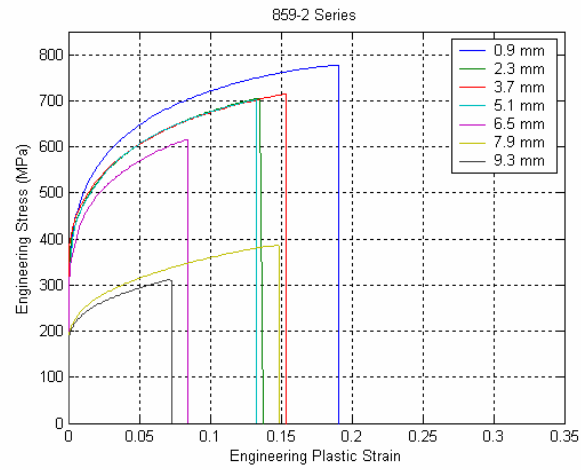
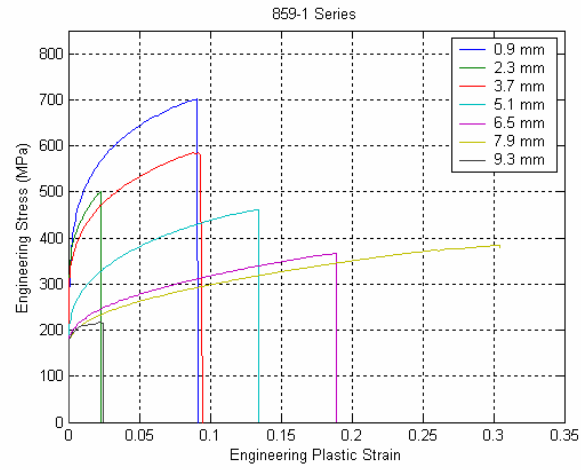
## D. 754 SERIES



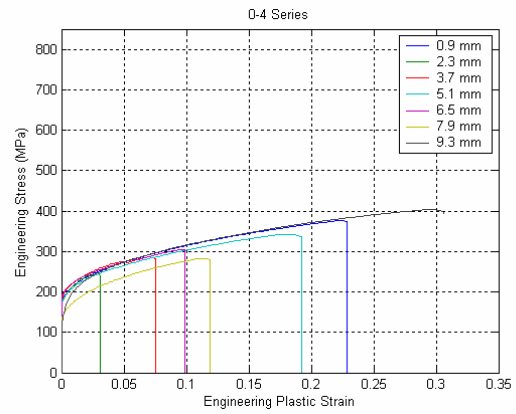
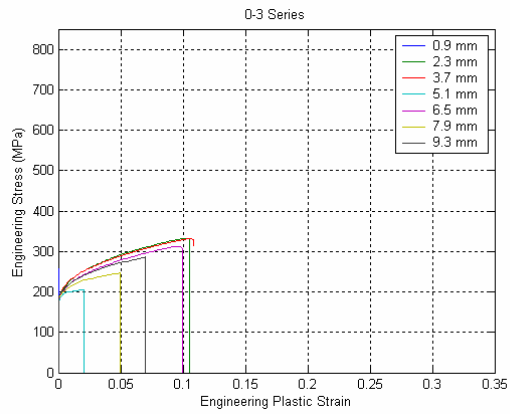
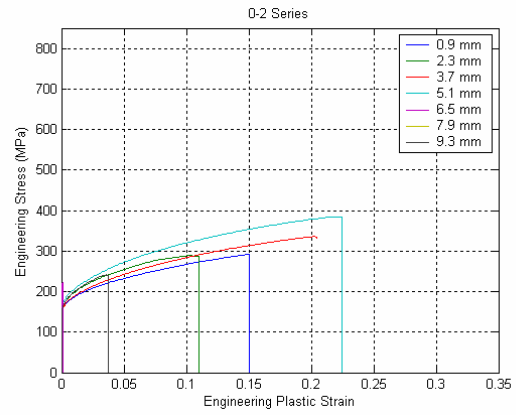
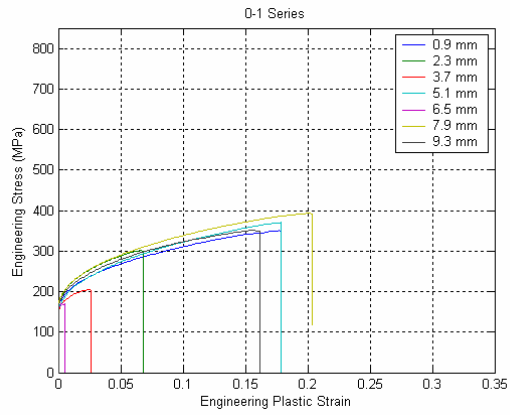
## E. 858 SERIES



## F. 859 SERIES



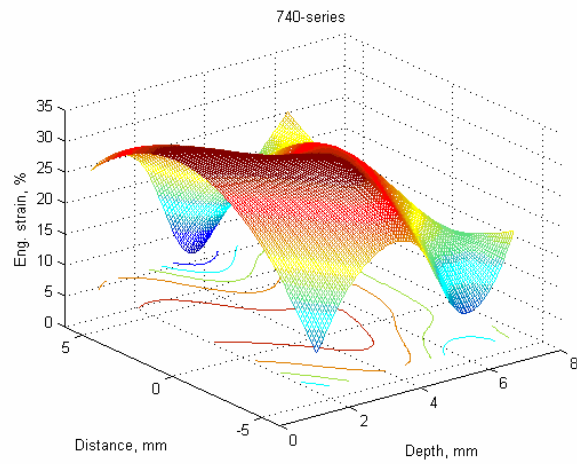
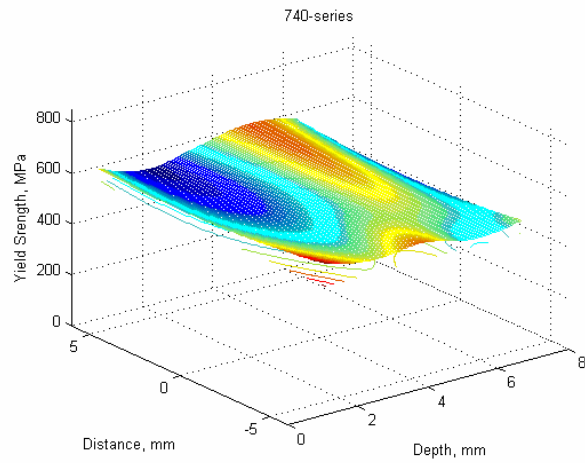
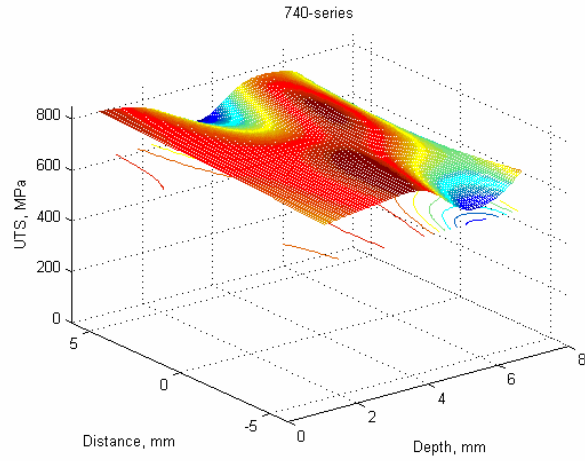
## G. BASE METAL SERIES



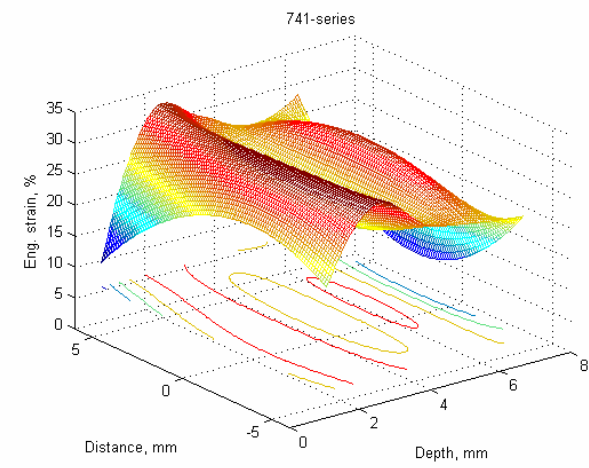
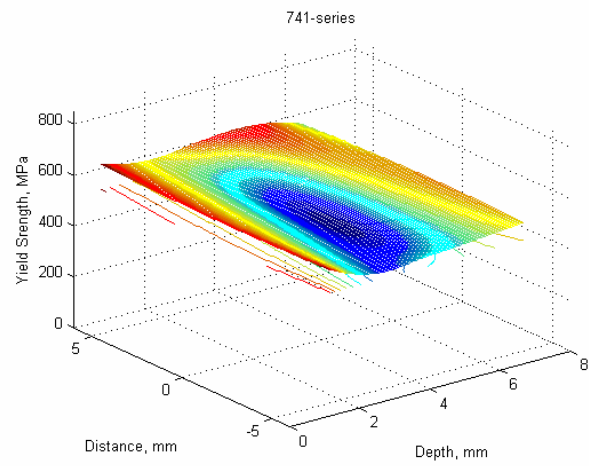
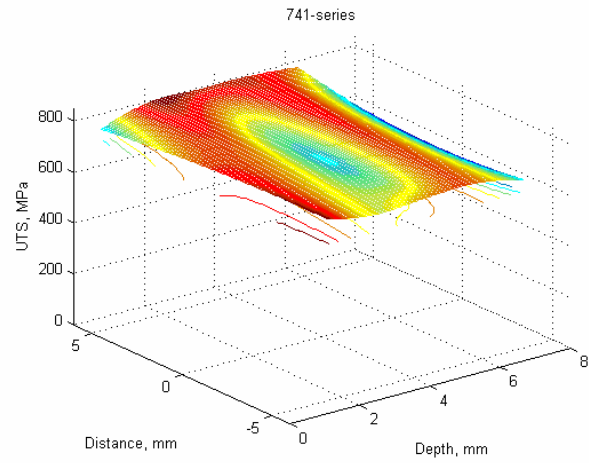
THIS PAGE INTENTIONALLY LEFT BLANK

## APPENDIX B – MESH AND CONTOUR PLOTS

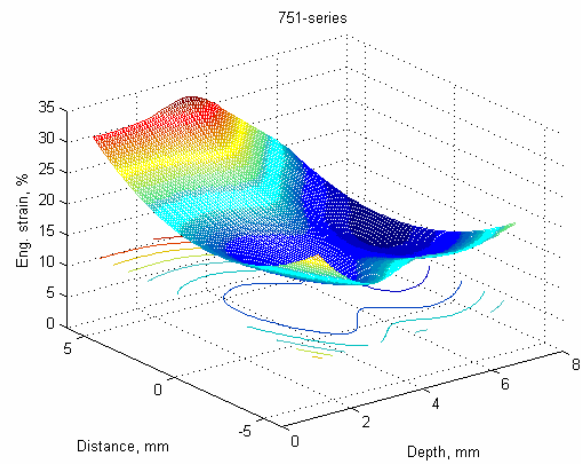
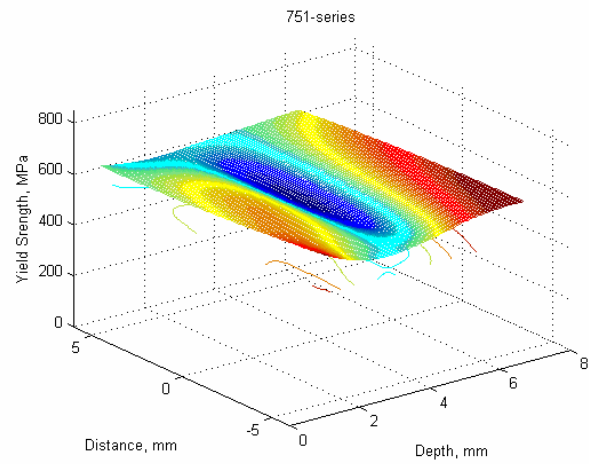
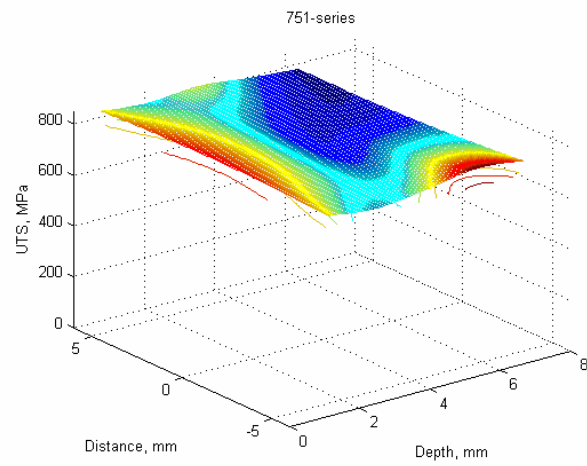
### A. 740 SERIES



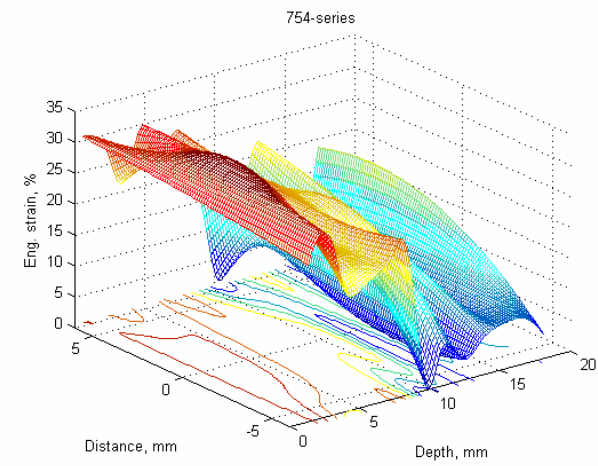
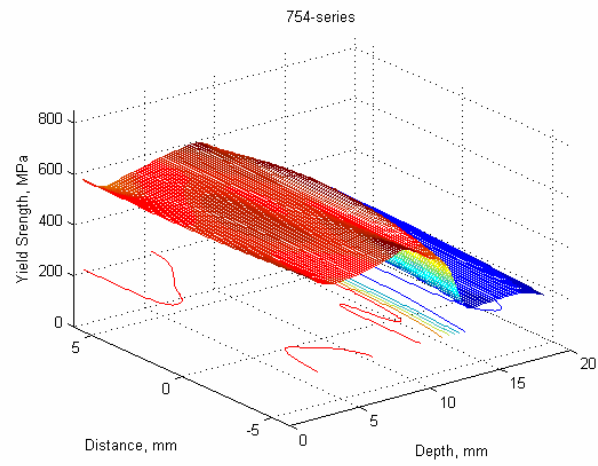
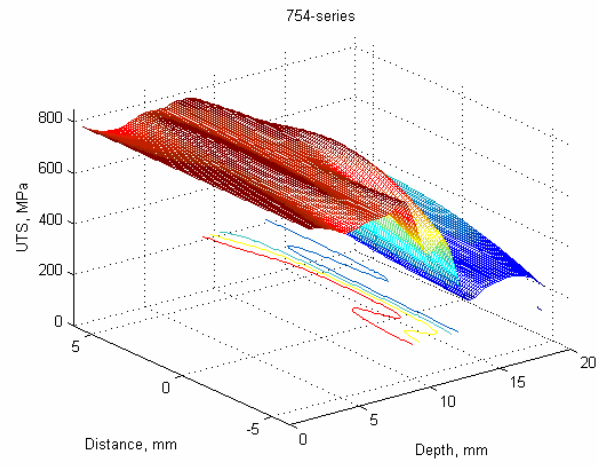
## B. 741 SERIES



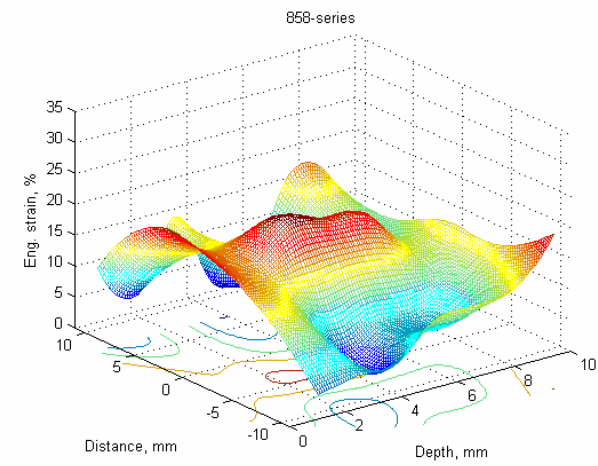
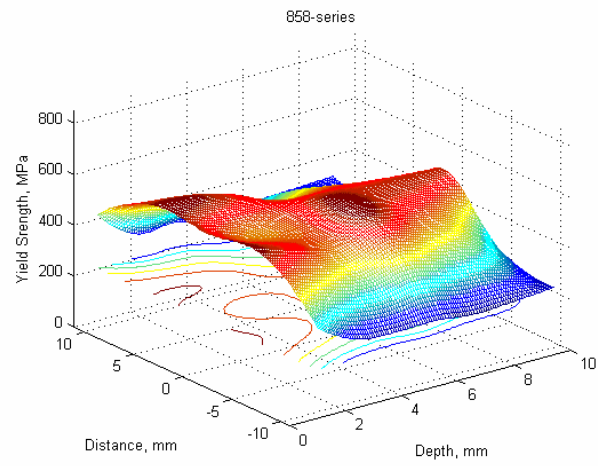
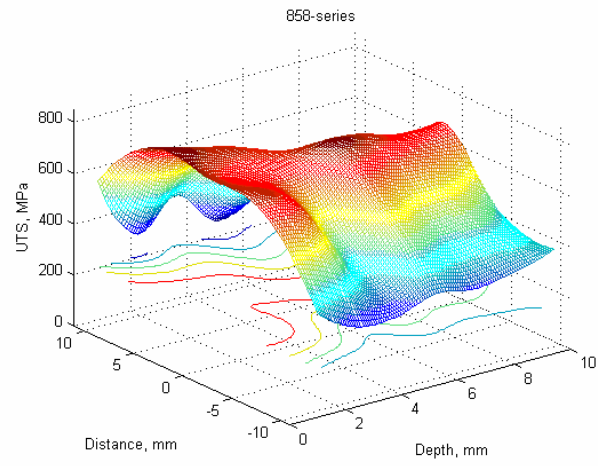
### C. 751 SERIES



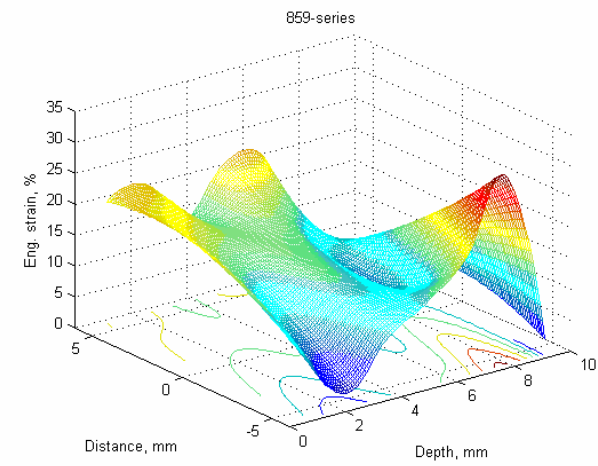
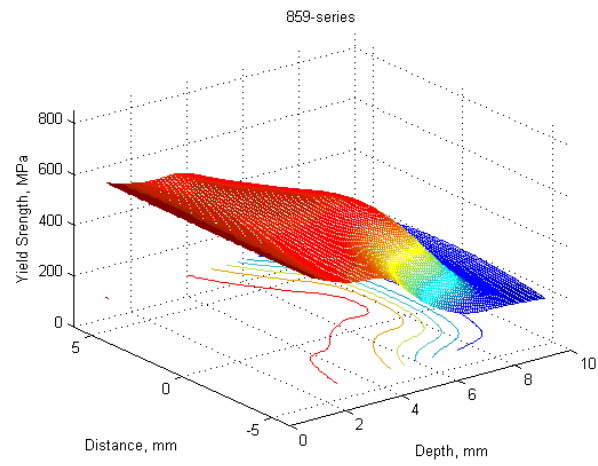
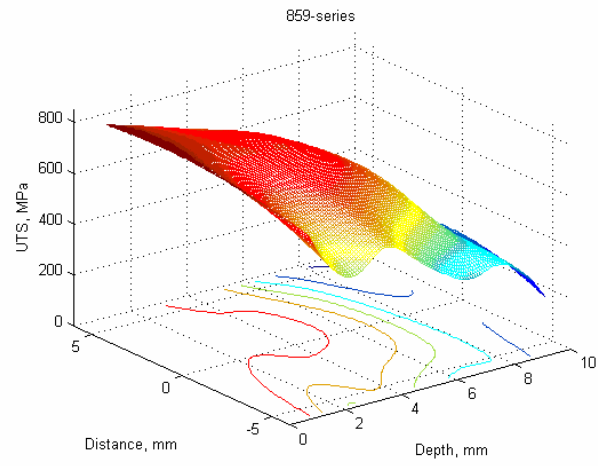
## D. 754 SERIES



## E. 858 SERIES



## F. 859 SERIES



## LIST OF REFERENCES

1. Mishra, R.S., *Advanced Materials and Processes*, v. 161(10), pp. 43-46, 2003
2. Mishra, R.S., Ma Z.Y., and Charit, I., *Mater. Sci. Engng. A*, v. A341, pp. 307-10, 2003
3. Ma, Z.Y., Mishra, R.S., and Mahoney, M. W., "Friction Stir Welding and Processing II", K.V. Jata, M.W. Mahoney, R.S. Mishra, S.L. Semiatin and T. Lienert, eds., TMS, Warrendale, PA, pp. 221-30, 2003
4. W. M. Thomas et. al., "Friction Stir Butt Welding", International Patent Appl. No. PCT/GB92/02203 and GB Patent Appl. No. 9125978.8, Dec 1991, U.S. Patent No. 5,460,317 – from [Ref. 2] in support of information by Stephan Kallee and Dave Nicholas TWI.
5. Rhodes, C. G. et al., "Effects of Friction Stir Welding on Microstructure of 7075 Aluminum," *Scripta Materialia*, v. 36, No. 1, p. 69-75, 1997.
6. Jata, K.V. and Semiatin, S.L., "Continuous Dynamic Recrystallization During Friction Stir Welding of High Strength Aluminum Alloys," *Scripta Materialia*, v. 43, p. 743-749, 2000.
7. Mishra, R.S. and Mahoney, M.W., "Friction Stir Processing: A New Grain Refinement Technique to Achieve High Strain Rate Superplasticity in Commercial Alloys," *Materials Science Forum*, v. 357-359, p. 507-514, 2001.
8. Sahoo, M., "Structure and Mechanical Properties of Slow-Cooled Nickel-Aluminum Bronze Alloy C95800," *AFS Trans*, v. 90, p. 913-926, 1982.
9. Culpan, E.A. and Rose, G., "Corrosion Behaviour of Cast Nickel Aluminium Bronze in Sea Water," *British Corrosion Journal*, v. 14, p. 160-166, 1979.
10. American Society for Testing and Materials (ASTM) B148 – 93a, Standard Specification for Aluminum-Bronze Sand Castings.
11. Sahoo, M., "Weldability of Nickel-Aluminum Bronze Alloy C95800," *AFS Trans*, v. 112, p. 893-911, 1982.
12. Wenschot, P., "The Properties of Ni-Al Bronze Sand Cast Ship Propellers in Relation to Section Thickness," *International Shipbuilding Progress*, v. 34, p.112-123, 1987.

13. Mahoney M. W., Bingel W. H., and Mishra R. S., "Microstructural Modification and Resultant Properties of Friction Stir Processed Cast NiAl Bronze" DARPA sponsored FSP website "Presentations and Publications"  
<http://www.darpa.mil/dso/thrust/matdev/fsp/prespub.html>  
Last access: 10 Sep 04
14. Nabach, W., Master's Thesis, "The Effects of Isothermal Deformation and Annealing on the Microstructure of Nickel-Aluminum-Bronze Propeller Material," Naval Postgraduate School, Monterey, CA, 2002.
15. Vasquez, B. K., MS Thesis, "The Effects of Isothermal Deformation and Annealing on the Microstructure of Nickel-Aluminum Bronze in Relation to the Friction Stir Process," Naval Postgraduate School, Monterey, CA, Dec 2002.
16. Pierce, F. A., MS Thesis, "The Isothermal Deformation of Nickel-Aluminum Bronze in Relation to the Friction Stir Processing," Naval Postgraduate School, Monterey, CA, Jun 2004.
17. Metals Handbook, 9<sup>th</sup> Ed., v. 2, Properties & Selections: Nonferrous Alloys and Pure Metals.
18. American Society for Testing and Materials (ASTM) E-8, Standard Test Methods for Tension Testing of Metallic Materials.
19. Oishi, K. and McNelley, T., "Microstructural Modification of As-Cast NiAl Bronze by Friction Stir Processing" *Metallurgical and Materials Transactions*, v. 35A in publication 2004.

## INITIAL DISTRIBUTION LIST

1. Defense Technical Information Center  
Ft. Belvoir, Virginia
2. Dudley Knox Library  
Naval Postgraduate School  
Monterey, California
3. Professor Terry McNelley  
Naval Postgraduate School  
Dept. of Mechanical Engineering  
Monterey, California
4. Professor A. J. Healey  
Naval Postgraduate School  
Dept. of Mechanical Engineering  
Monterey, California
5. CDR S. Cunningham  
Naval Postgraduate School  
Dept. of Mechanical Engineering  
Monterey, California
6. Murray W. Mahoney  
Rockwell Science Center  
Thousand Oaks, California
7. William Palko  
Naval Surface Warfare Center  
Caderock Division  
West Bethesda, Maryland
8. Dr. Leo Christodoulou  
DARPA/DSO  
Arlington, Virginia